Evaluation of parameterization schemes for matric potential in frozen soil in land surface models: A modeling perspective

Yi Zhao[1], Zhuotong Nan[1,2*], Zetao Cao[1], Hailong Ji[1], Jianan Hu[1]

[1]Key Laboratory of Ministry of Education on Virtual Geographic Environment, Nanjing Normal University, Nanjing, 210023, China

[2]Jiangsu Center for Collaborative Innovation in Geographical Information Resource Development and Application, Nanjing, 210023, China

Corresponding author: Zhuotong Nan (nanzt@njnu.edu.cn)

Key points:

- Four schemes parameterizing soil matric potential with different effects of pore ice were evaluated from a modeling perspective.
- Schemes with partial ice effects performed worse than those with both or no ice effects in simulating active layer dynamics.
- Scheme considering both effective porosity and cryosuction functioned best in simulating phase change and soil liquid content.

How to cite:

Zhao Y, Nan Z, Cao Z, Ji H, Hu J. Evaluation of parameterization schemes for matric potential in frozen soil in land surface models: A modeling perspective. Water Resources Research. 2023, 59(6): e2023WR034644. doi:10.1029/2023WR034644.

Abstract

Soil matric potential (SMP) is an important variable in land surface models (LSMs) for regulating soil hydrological processes and highly influenced by soil ice in frozen ground. In this study, four SMP parameterization schemes that incorporate different effects of soil pore ice were separately integrated into the Simultaneous Heat and Water (SHAW) model and evaluated for their ability to simulate heat and water transport at a permafrost monitoring site at the Tanggula Mountain Pass on the inner Qinghai-Tibet Plateau based on the same data and model settings. The schemes differed in their treatment of pore ice effects, including effective porosity and cryosuction. An identifiability analysis of SMP-related parameters for each scheme was performed, based on 1000-fold random parameter sampling. The scheme that considered both effects performed best, accurately simulating both soil moisture content and temperature in the active layer. The schemes that considered only one effect of pore ice showed limitations, with the effective porosity scheme underestimating unfrozen water content and the cryosuction scheme seriously overestimating it, and both schemes leading to large discrepancies in simulated soil temperature. The scheme that ignored both effects performed better than the partially considered schemes due to a compensating effect of reduced effective porosity and increased cryosuction in the presence of pore ice, but not as well as the scheme that considered both effects, particularly in simulating soil temperature during freezing periods and estimating unfrozen water content near the mid-depth of the active layer.

Plain Language Summary

Soil matric potential (SMP) is a measure of how tightly water is held in the soil, and is an important factor in describing soil hydrology. In cold regions, pore ice can affect SMP in two ways: by occupying soil pores, which weakens the SMP, or by adsorbing surrounding liquid, which strengthens the SMP. This study compared four SMP equations that include different effects of pore ices in a model of heat and water transport. The equations were implemented in the Simultaneous Heat and Water model and tested using the same dataset from a permafrost site on the Qinghai-Tibet Plateau. The results showed that the equations that only considered one effect led to significant errors in simulating frozen ground. The equation that ignored both effects performed better than the partially considered equations because of the tradeoff between the two effects, but still had deficiencies in simulating thawing processes and overestimating unfrozen water content at the intermediate soil depth. The equation that considered both effects performed the best and thus is recommended to be included in models for permafrost regions.

1 Introduction

The Northern Hemisphere contains vast areas of permafrost, including high-latitude pan-Arctic regions and mid-latitude mountainous regions like the Qinghai-Tibet Plateau (QTP)(Obu, 2021; Zhang et al., 2000). Pore ice is widely present in permafrost active layers, seasonally frozen soils, and the frozen layers around supra-permafrost taliks in cold regions. It plays a crucial role in soil heat and water dynamics by affecting surface and subsurface water exchange, storage, and routing (Boike et al., 1998; Walvoord & Kurylyk, 2016), as well as thermal properties such as specific heat capacity, thermal conductivity and latent heat (Akyurt et al., 2002; He et al., 2021). With global climate warming, significant permafrost degradation has occurred, leading to altered local hydrology and terrestrial ecosystem due to ground ice thaw (Liljedahl et al., 2016; Smith et al., 2022). Therefore, a comprehensive understanding of pore ice's role in controlling soil water migration and distribution is crucial for predicting hydrological and thermal dynamics, environmental changes, and climate feedbacks in areas affected by frozen ground. As a powerful tool for understanding the exchange of heat and water and their response to climate changes in permafrost regions (Blyth et al., 2021), land surface models (LSMs) have evolved to consider the impacts of soil ice, such as reduction in permeability (Azmatch et al., 2012; Chen et al., 2021; Watanabe & Osada, 2017), freezing point depression (Li et al., 2010), and changes in thermal properties (Kurylyk & Watanabe, 2013), to represent soil hydrological and thermal processes in permafrost regions more accurately.

Soil matric potential (SMP) is an important hydraulic variable that regulates soil water distribution and fluid migration in LSMs. It refers to the tenacity with which water is held by the soil matric (Mullins, 2000). SMP is strongly affected by the multiple impacts of pore ice (Xue et al., 2021), which include cryosuction and the reduction of effective porosity. Cryosuction occurs when the SMP increases as the unfrozen water content (UWC) decreases during the ground freezing process. This process results in the migration of liquid water from the unfrozen soil to the freezing fronts (Cheng, 1983; Kane & Stein, 1983). Laboratory observations have confirmed the increase in SMP during soil freezing (Wen et al., 2012; Xue et al., 2021). Many empirical or physically-based approaches have been developed to represent cryosuction in soil freezing (Dall'Amico et al., 2011; Hu et al., 2020; Painter, 2011). Among them, a physically-based approach for SMP estimation proposed by Kuilk (1978) improved the Campbell SMP equation (Campbell, 1974) with an additional term representing cryosuction. This approach has been widely applied in model simulation studies in cold regions (Koren et al., 1999; Li et al., 2010; Stuurop et al., 2021; Wang et al., 2017; Wang et al., 2021; Zhang et al., 2007). The increased constituent of soil ice also affects the soil water potential by reducing the soil pores, but the latest modeling studies have not yet incorporated this effect. The only exceptions are the Community Land Model (CLM) and Common Land Model (CoLM), which incorporate a revised SMP scheme

that determines soil wetness from effective porosity by excluding the volume of soil ice from the total soil porosity (Dai et al., 2001; Dai et al., 2003; Oleson et al., 2013).

Differences in SMP representations are one of the important structural differences among models or parameterizations for soil hydrology (Andresen et al., 2020; Slater & Lawrence, 2013). However, the performance of these representations in real-world applications of LSMs, particularly in cold regions, is yet unclear. While some studies (Ganji et al., (2017) and Zheng et al., (2017)) have evaluated the performance improvement in a model setting by including the cryosuction effect in the current SMP schemes, there remains a pressing need for a comprehensive and unbiased evaluation of different SMP schemes with varying physical representations of soil ice within an LSM framework. Although the CLM and CoLM are widely used in research on cold regions (Guo & Wang, 2013; Hermoso De Mendoza et al., 2020), the SMP parameterization in CLM and CoLM, which includes the effect of effective porosity, has been found to underestimate the UWC than those without (Xiao et al., 2013). Given the increasing applications of LSM in the simulation of permafrost dynamics, it is crucial to have a clear picture of the performance of these ice-included SMP schemes and the mechanisms behind their performance.

However, evaluating current SMP schemes faces two main challenges. Firstly, these SMP schemes are typically coupled with LSMs that differ in methodology, model structure, and input requirements, and they are from diverse geotechnical and hydrological backgrounds (Kurylyk & Watanabe, 2013). Model simulation based comparisons of SMP parameterizations are thus impaired by many factors, such as the differences in model structure and model inputs (Andresen et al., 2020; Liu et al., 2020). Secondly, even with model differences eliminated, an unbiased evaluation must take proper account for the identifiability of parameters and the optimal parameter-value space intrinsic to each SMP parameterization. This is crucial because uncertainties in soil parameters can contribute significantly to the simulation results, such as soil temperatures and moisture contents (Harp et al., 2016), thereby compromising the conclusion of their performance. Each new parameter introduced into an existing SMP parameterization represents a new dimension of parameter space, and will lead to increased difficulty in parameter identifiability (Beven, 2006; Kirchner, 2006) and consequently to a change in the optimal parameter-value space. Recent studies have highlighted the importance of sound parameter uncertainty analysis for LSMs in arriving at a thorough evaluation of the parameterization schemes by isolating them from the influence of parameter uncertainty (Mai et al., 2022; Yoshida et al., 2022).

Given the limitations of existing studies, a comprehensive evaluation of the different SMP schemes considering the effects of pore ice is still missing, making it difficult to determine which SMP parameterization is more suitable for frozen ground. This study aims to address the gap by assessing four SMP schemes with different representations of soil ice in reproducing soil water and heat dynamics in a permafrost area. The evaluation and parametric uncertain analysis were performed based on

ensemble simulations with 1000 random parameter sets generated by the Latin hypercube sampling method. The specific objectives are to quantify the performance of the different ice-included SMP schemes and the uncertainties associated with them in simulating permafrost heat and water dynamics, and to provide new insights into the mechanisms behind the performance of the different SMP schemes.

To achieve these objectives, the four SMP schemes were each incorporated into the Simultaneous Heat and Water (SHAW) model (Flerchinger & Saxton, 1989a), a 1D heat, water and solute transfer model. The SHAW models were then driven by the same forcing data from a permafrost monitoring site at the Tanggula (TGL) Mountain Pass site along the Qinghai-Tibet Highway on the inner Qinghai-Tibet Plateau (QTP) to minimize disturbances beyond the SMP schemes themselves. The study will propose a more appropriate SMP scheme for cold regions based on the evaluation results.

2 Methodology and data

2.1 Experimental area and data

The Tanggula (TGL) site (33°04′ N and 91°56′ E) is a typical permafrost site located on a southwest slope of the Tanggula Mountains on the inner QTP (Figure 1a). This site has been extensively studied for permafrost research, including the evaluation of LSMs (Hu et al., 2015; Li et al., 2020), permafrost heat and water dynamics (Li et al., 2019), and the response of permafrost to climate change (Zhu et al., 2017; Zhu et al., 2021). The site is notable for its quality-controlled, long-term observations of soil temperature and moisture content, and hourly meteorological observations, which are available for analysis (Zhao et al., 2021). The TGL site has an elevation of approximately 5100 m above sea level (a.s.l.), and the soil texture is primarily loamy sand according to the USDA classification (2017). The local vegetation cover consists of sparse alpine meadows with a coverage fraction of approximately 30– 40%. The annual average air temperature is −4.9 °C, and the active-layer thickness (ALT) is about 3 m (Xiao et al., 2013). The annual precipitation is around 400 mm, with 92% occurring from May to September.

The automatic weather station installed at the TGL site collects meteorological data at 2 m height, including hourly air temperature, wind speed, relative humidity, downward shortwave radiation, and precipitation (Figure 1b). Additionally, a monitoring system records soil temperature and UWC at depths ranging from 0.05 to 2.8 m below the ground surface, with measurements taken at 11 different depths (0.05, 0.1, 0.2, 0.4, 0.7, 1.05, 1.3, 1.75, 2.1, 2.45 and 2.8 m). Compared to other permafrost sites on the QTP, the TGL site has the advantage of providing hourly meteorological data and daily observations of the whole profile of the permafrost active layer.

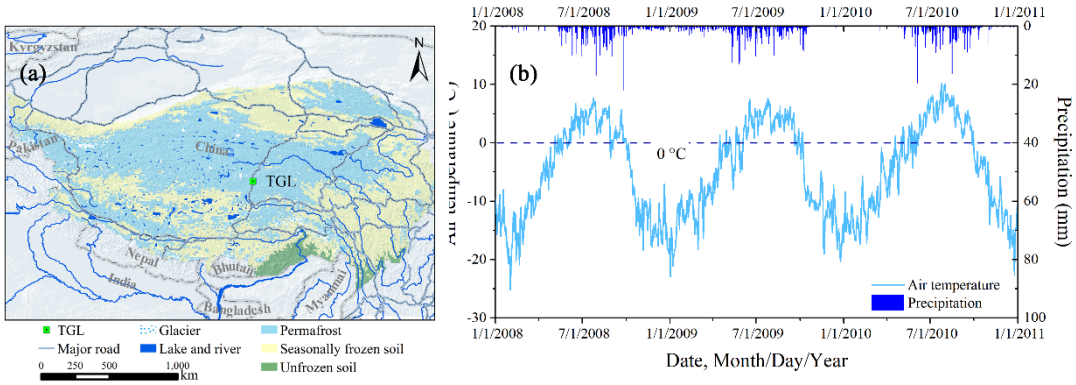

Figure 1 The map (a) showing the location of the Tanggula (TGL) permafrost site, as well as the air temperature and precipitation (b) at the site. Time series of daily air temperature at 2m height and precipitation were aggregated from the hourly measurements. The base map of permafrost distribution on the Qinghai–Tibet plateau (QTP) is from Zou et al. (2017).

2.2 Parameterizations of frozen soil matric potential

There are several forms of SMP parameterization, such as the Campbell method (Campbell, 1974), Brooks-Corey equation (Brooks, 1964), and van Genuchten equation (van Genuchten, 1980). This study focuses on the Campbell-based SMP scheme and its variants for permafrost applications. Other forms are discussed in the discussion section. The Campbell method does not take into account the effect of pore ice. It defines SMP (Ψ) as being related to volumetric liquid water content and soil hydraulic properties:

$$\Psi = \Psi_e \left(\frac{\theta_l}{\theta_s}\right)^{-b} \quad (1)$$

where Ψ_e is the air entry potential (m), which controls the shape of the soil water retention curve, θ_l and θ_s are the liquid water content and porosity ($m^3 \cdot m^{-3}$) of the soil, and b is a parameter for pore size distribution.

Since the Campbell method was originally developed for non-frozen soils, its applicability and performance in cold region applications could be questionable (Li et al., 2010) as the SMP of frozen soils is strongly controlled by the ice content (Xue et al., 2021). SMP is closely related to normalized soil wetness, which is determined as a percentage of liquid water in the soil pore space. As the pore ice content increases and occupies the free pore space, the effective pore space for liquid water decreases, and the SMP can be significantly influenced. Thus, the SMP equation has been improved by accounting for this effective porosity of the soil, which is defined as $(\theta_s - \theta_i)$, where θ_i is the ice content ($m^3 \cdot m^{-3}$), as implemented in the CLM 4.5 (Oleson et al., 2013) and CoLM (Dai et al., 2001) models. The improved SMP scheme considering effective porosity is thus formulated as:

$$\Psi = \Psi_e \left(\frac{\theta_l}{\theta_s - \theta_i}\right)^{-b} \quad (2)$$

Cryosuction, described as an increase in matric suction in frozen soils with growing ice content, represents another important effect of soil ice that results in the migration of soil moisture from the adjacent unfrozen layer to the freezing front. An equation for incorporating cryosuction into the Campbell method was developed by Kulik (1978) :

$$\Psi = \Psi_e \left(\frac{\theta_l}{\theta_s}\right)^{-b} (1 + C_k \theta_i)^2 \quad (3)$$

where C_k represents the effect of soil specific surface on matric potential due to the presence of ice, and an average value of 8 was suggested (Kulik, 1978).

Eqs. 2 and 3 improve the original Campbell method in different aspects, but mathematically contradict each other in estimating the value of frozen soil SMP. The SMP estimated by Eq. 2 is expected to be smaller than the results of the original Eq.1, given the same unfrozen water and ice contents and soil characteristics, while that of Eq. 3 is much larger than that of Eq. 1. Since both of these effects simultaneously control the frozen SMP, we proposed a new scheme considering the merging of the effects of effective porosity and cryosuction:

$$\Psi = \Psi_e \left(\frac{\theta_l}{\theta_s - \theta_i}\right)^{-b} (1 + C_k \theta_i)^2 \quad (4)$$

2.3 The Simultaneous Heat and Water (SHAW) model and scenario design

Previous studies have evaluated the performance of SMP parameterization schemes, focusing on only one effect of effective porosity (Eq. 2) or cryosuction (Eq. 3) in cold regions (Hu et al., 2020; Xiao et al., 2013; Zhang et al., 2007). However, inter-comparison between the SMP schemes and how they work in permafrost settings remained unclear, as the evaluations were made using different models, data and model configurations. In this study, to minimize the disturbance coming from confounding factors, each of the three previously developed SMP schemes (Eqs. 1-3) and the proposed one (Eq. 4) were incorporated into a uniform heat and water transfer model framework, i.e., the Simultaneous Heat and Water (SHAW) model, by modifying the related model codes. By leaving the other processes unchanged and driving the models with the same data and model settings, it is possible to fairly compare the four SMP schemes and demonstrate the impact of each scheme on the simulated soil water dynamics, as well as concomitant soil temperature.

The SHAW model considers elaborate physics of the interconnected water and heat exchange processes within frozen ground, including the mechanisms of latent heat, convective heat from vapor and liquid water migration, and the effects of soil ice on soil permeability (Flerchinger et al., 2012; Flerchinger & Saxton, 1989a), making it advantageous for exploring the complex interactions among climate, landscape and permafrost dynamics. Numerous applications of the SHAW model have proven its satisfactory performance in cold regions (Flerchinger & Pierson, 1997; Flerchinger &

Saxton, 1989b), covering a wide spectrum of topics, such as permafrost evolution (Wei et al., 2011), freeze-thaw cycle characteristics (Chen et al., 2019; Cui et al., 2020), and permafrost responses to climate and land ecosystem changes (Huang & Gallichand, 2006; Kahimba et al., 2009; Link et al., 2004; Zuo et al., 2019). Our previous study (Zhao et al., 2022) on a SHAW simulation at the TGL site showed that the simulation accuracy of soil temperature and moisture content can exceed 0.7 and 0.4, respectively, in terms of the Nash-Sutcliffe coefficient of efficiency (NSE) at most active layer depth, indicating the satisfactory performance of the SHAW model at the TGL.

The soil moisture diffusion equation for each soil layer in the SHAW model is given by Eq. 5:

$$\frac{\partial}{\partial z}\left[K\left(\frac{\partial \Psi}{\partial z}+1\right)\right]+\frac{1}{\rho_l}\frac{\partial q_v}{\partial z}+U=\frac{\partial \theta_l}{\partial t}+\frac{\rho_i}{\rho_l}\frac{\partial \theta_i}{\partial t} \quad (5)$$

where ρ_i and ρ_l are the densities of ice and liquid water ($kg \cdot m^{-3}$), respectively; θ_i and θ_l are the volumetric ice and UWC of the soil layer ($m^3 \cdot m^{-3}$), respectively; q_v is the liquid water flux ($m \cdot s^{-1}$); U is a source/sink term for water uptaken by roots ($m^3 \cdot m^{-3} \cdot s^{-1}$); t and z represent the time step and the center depth of the soil layer, respectively. Ψ is the SMP (m) estimated from Eq.1. K is the vertical conductivity ($cm \cdot h^{-1}$), and it can be given by Eq. 6:

$$K=K_s\left(\frac{\Psi_e}{\Psi}\right)^{\left(2+\frac{3}{b}\right)} \quad (6)$$

where K_s is the saturated vertical conductivity ($cm \cdot h^{-1}$). When the soil temperature is below 0 ° C and ice is present, the total soil matric pressure is determined by a simplified Clausius-Clapeyron equation (Eq. 7):

$$\emptyset=\Psi+\pi=\frac{L_f}{g}\left(\frac{T}{T_K}\right) \quad (7)$$

where $\emptyset$ is the total soil water potential, Ψ is the SMP calculated from Eq.1, π is osmotic potential (m) which is ignored in this study given its minor influence, g is the acceleration due to gravity ($m \cdot s^{-2}$), L_f is the latent heat of fusion ($kJ \cdot kg^{-1}$), T is the soil temperature, and T_K is T in Kelvins. The UWC and ice content at a temperature below the freezing point can be expressed by combining Eqs.1 and 7:

$$\frac{L_f}{g}\left(\frac{T}{T_K}\right)=\Psi_e\left(\frac{\theta_l}{\theta_s}\right)^{-b} \quad \rightarrow \quad \theta_l=\theta_s\left(\frac{L_f T}{\Psi_e g T_k}\right)^{-\frac{1}{b}} \quad (8)$$

$$\theta_i=(\theta_w-\theta_l)\frac{\rho_i}{\rho_l} \quad (9)$$

where θ_w is the total water equivalent in a soil layer.

In Eq.8, the potential of frozen soil is calculated by the Clausius-Clapeyron equation, which takes into account the total potential caused by pore ice. However, the original Campbell equation only represents the potential of unfrozen water, resulting in

unequal sides of Eq.8. In this study, we aimed to incorporate the impacts of pore ice into the SMP parameterization by replacing Eq. 1 in the SHAW model with Eqs. 2, 3 and 4, respectively. As a result, we created four different SHAW models to represent scenarios with varying degrees of impact of soil ice on the SMP: (1) Baseline: using the original SHAW SMP parameterization scheme (Eq. 1) without considering the effect of soil ice in SMP estimation; (2) P: using a modified scheme based on Eq. 2, which considers effective porosity; (3) ICE: using a modified scheme based on Eq. 3, which represents the effect of cryosuction; and (4) P+ICE: using a modified scheme based on Eq. 4, which considers both effective porosity and cryosuction. All four model scenarios were run with the same forcing data, initial and boundary conditions, and parameters. As the only difference among the four models is the choice of SMP schemes, any differences between the simulations can be attributed to the exclusive contributions of the SMP schemes.

2.4 Model configurations

The SHAW model and its variants were driven by hourly meteorological data in 2008-2010 from the TGL site. As there was a lack of in-situ snow density observation, the models estimated new snow density based on the air temperature of each time step. The vertical discretization of the soil column consisted of 13 layers, most of which matched the measurement depths. A special zero-depth layer was added to represent the interface between the dead plant residue layer and the soil column. The depths of the soil layers and the texture of each layer are presented in Table 1. To fit the complex coupled water-heat exchange processes and sub-time step iteration scheme of the model, an accurate lower boundary condition at a shallow depth is necessary (Chen et al., 2019; Cui et al., 2020; Flerchinger, 1991; Marshall et al., 2021). Therefore, in this study, we used the fluctuating daily soil temperatures measured at the 2.8 m depth, which was the closest layer to the base of the active layer, as the lower boundary temperature condition to constrain heat fluxes through this depth. The soil water equivalents (including both ice and liquid water) at the lower boundary were determined separately for thaw (temperature > 0 ° C) and freeze (temperature ⩽ 0 °C) periods. During thaw periods, the observed water content was directly used as the lower hydraulic condition. However, for freeze periods where the total water equivalent could not be obtained by observations, we set the lower boundary water content to a fixed value of 0.25 m^3 m^{-3}. This value was determined based on observations during the thaw periods, where the water content first rose due to percolation from upper layers and then stabilized at 0.25 m^3 m^{-3}. The SHAW model then automatically determined the ice and liquid water contents depending on the temperature at the lower boundary depth. Before the formal simulation, each model simulation was subjected to an individual “spin up” period of three decades by repeating the forcing data from 2008 to 2010. This process was necessary to minimize the uncertainties caused by inaccurate initial conditions of soil temperature and moisture (Ji et al., 2022).

Table 1 Stratification of the soil column, composition of soil grain size, and bulk density, ρ_b, of the soil profile at the Tanggula site (TGL).

Depth of soil node (m)	Sand (%)	Silt (%)	Clay (%)	ρ_b ($g \cdot cm^{-3}$)
0.00	93	1	6	1176
0.02	93	1	6	1176
0.05	93	1	6	1176
0.10	93	1	6	1176
0.20	87	3	10	1331
0.40	89	2	9	1103
0.50	87	3	10	1405
0.70	84	3	13	1405
1.05	75	7	18	1235
1.30	75	7	18	1281
1.75	71	8	21	1253
2.10	71	8	21	1460
2.45	71	8	21	1332

2.5 Parametric identifiability analysis and performance criteria

Parameter identifiability analysis in this study assesses whether it is theoretically possible to estimate unique parameter values from data and evaluates how the optimal parametric space varies across different SMP schemes. To accomplish this, we conducted an uncertainty analysis on these four soil hydraulic parameters that play a critical role in determining the SMP. These parameters include the saturated water content, air entry potential, pore size distribution, and the saturated vertical hydraulic conductivity. This analysis also enhances our understanding of the sensitivity of the SMP schemes and reduces the potential for performance bias based on a single set of parameter values, as commonly in prior studies (Stuurop et al., 2021; Zhang et al., 2007; Zheng et al., 2017).

We used the Latin hypercube sampling method to generate 1000 random sets, with the effective ranges of the parameters (Table 2) determined based on existing literature (Chen et al., 2019; Liu et al., 2013; Wu et al., 2018). As the proximal soil layers are more similar in texture than those further apart, a base value for each parameter was generated for each of the 1000 times, and then the base values were randomly fluctuated within a 5% margin of their values before being assigned to each soil layer. This approach ensured that the parameter values for all soil layers were sufficiently random while maintaining the continuity of a real soil column.

Table 2 Soil hydraulic parameters related to the studied soil matric potential (SMP) schemes and their predetermined ranges

Parameter	Notation (Units)	Predetermined range
Saturated vertical hydraulic conductivity	$\boldsymbol{K_s}$ $(\mathrm{cm \cdot h^{-1}})$	0.01 ~ 100
Saturated water content	$\boldsymbol{\theta_s}$ $(\mathrm{m^3 \cdot m^{-3}})$	0.3 ~ 0.6
Air entry potential	$\boldsymbol{\psi_e}$ (m)	−0.5 ~ −0.2
Pore size distribution	$\boldsymbol{b}$	3.5 ~ 5

To provide a comprehensive understanding of the heterogeneous heat and water dynamics in the different depths of the active layer, we selected three representative soil layers, i.e., a layer at 0.05 m depth closest to the ground surface where observations are available, a layer at 0.4 m depth located in the middle of the soil strata that is less affected by both the upper and lower boundaries, and a layer at 2.45 m approaching the bottom of the active layer. There three layers were chosen to represent typical conditions at the near surface, middle and lower part of the active layer, respectively.

It should be noted that the other model parameters were not exposed to uncertainty analysis, and their values were determined based on the TGL conditions with reference to our previous study (Zhao et al., 2022). Additionally, as the original SHAW model did not specify a residual UWC when using the Campbell scheme, we defined a minimum liquid content of 0.02 $\mathrm{m^3 \cdot m^{-3}}$ as a threshold to avoid the occurrence of extremely low UWC simulated by the modified schemes. By running the ensemble of the four model scenarios based on these 1000 parameter sets, we were able to evaluate the overall performance and parameter-induced uncertainties associated with the different SMP schemes at TGL. The following criteria were utilized to evaluate the performances of the four SMP schemes at the selected depths:

(1) Computational stability of the SHAW variants, which differ only in the SMP scheme. The inclusion of inappropriate physical constraints in a numeric model can adversely affect the model's stability (Schoups et al., 2008). In this study, a valid simulation is defined as one that can be run, without interruptions due to failure in convergence during iterations, for the entire spin-up and subsequent simulation periods, given a specified set of parameter values. Hence, the number of valid simulations out of 1000 simulations relative to the 1000 random parameter sets is used to estimate the computational stability of a model and the usability of the employed SMP scheme. Any simulations that are numerically unstable but do not interrupt are retained to track the flaws of the associated scheme. In case a very small number of valid simulations is found for a modified model, the total number of simulations is augmented to 3000 to obtain an adequate number of valid simulations for subsequent analysis.

(2) Simulation accuracies at the three selected soil depths (0.05, 0.4 and 2.45 m). The performances of the implemented SMP schemes are assessed based on a range of NSE values computed for soil temperature/moisture content simulations of each depth, using the ensemble run results of a scenario against the observations. The NSE values reflect the model's ability to simulate the observations accurately. The NSE is defined as:

$$\mathrm{NSE} = 1 - \frac{\sum_{t=1}^{N}(O^t - M^t)^2}{\sum_{t=1}^{N}(O^t - \bar{O})^2} \quad (10)$$

where O^t and M^t are the observed value and the simulated value at time t; $\bar{O}$ is the mean of the observations over the entire period; and N is the total number of time steps. The behavioral parameter space that results in high simulation accuracy is recorded for each scenario to explore parameter identifiability associated with each SMP scheme.

(3) Ninety-five percent prediction uncertainty (95PPU) band for simulated soil temperature/moisture content. The 95PPU bands for each scenario are calculated at the 2.5% to 97.5% levels of the simulated values of soil temperature/moisture content from all valid simulations of this scenario. These bands indicate the spread range of the model outputs in response to changes in the variable parameters. A 95PPU band that essentially encompasses the observations and is normally distributed around the observations reflects good model performance. Conversely, a 95PPU band that cannot capture the observation trend reflects large errors contained in the simulation (Yang et al., 2008).

3 Results

3.1 Model stability and simulation accuracies

The SMP schemes in the Baseline (no effects considered) and P (effective porosity considered) scenarios were numerically stable, yielding 992 and 998 valid simulations out of the 1000 total simulations with random parameter sets, respectively. However, only 159 valid simulations were obtained for the ICE (cryosuction considered) scenario, indicating that the inclusion of cryosuction negatively affected the model stability. To achieve an adequate number of valid simulations for analysis, the sampling size for the ICE scenario was increased to 3000, and finally 374 valid simulations were obtained. The P+ICE (both effects considered) SMP scheme was also affected by the negative impacts of cryosuction, but the consideration of effective porosity in this scheme may mitigate model instability, resulting in 622 valid simulations out of 1000.

For the Baseline scenario, most of the NSE values measured between the simulated soil temperatures (moisture content) and the observed ones exceeded 0.7 (0.4) at each depth, respectively (Figure 2), except for the NSEs for soil moisture content at 0.4 m depth (Figure 2 e), where most values were negative. This suggests that the original Campbell method can broadly simulate soil temperature and moisture content, even if the effects of soil pore ice are completely ignored.

The NSE boxplots of simulated soil temperature in the P scenario were more widely spread at all depths, and had generally lower positions, much lower minima and 1st percentile values than those of the Baseline (Figure 2 a-c). Regarding soil moisture simulation, the NSEs for P were also lower than those of the Baseline at the ground surface (0.05 m) and bottom depths (2.45 m) (Figure 2 d, f). Especially at 2.45 m, the mean of NSE for soil moisture simulation with P was significantly lower than the

409 median of NSE, indicating some extremely poor soil moisture simulations under the P
410 scenario at this depth. However, a reversed trend was found at 0.4 m depth, where P
411 simulated better for soil moisture than the Baseline, as evidenced by the higher
412 interquartile range (IQR), mean and median values, and the bottom edge of the NSE
413 box in the P scenario (Figure 2 e).

414 Among all scenarios, the ICE scenario stands out as having the widest IQR, and
415 the lowest mean and median values of NSE for simulations of both soil temperature and
416 moisture at all depths. Although some simulations in the ICE scenario had maximum
417 NSE values and 99th percentile comparable to other scenarios, the majority of
418 simulations resulted in very low NSE values (Figure 2 d-f, with truncated extremely
419 low NSEs for legibility), showing poor performance of the SMP scheme with only the
420 effect of cryosuction considered. The generally inferior performance of the P and ICE
421 scenarios compared to the Baseline underscores that the partial inclusion of soil ice
422 effects in the SMP equation falls well short of what is necessary to improve the
423 simulation of freezing and thawing processes. Despite their widespread use in previous
424 studies, partially considered SMP schemes may lead to performance degradation rather
425 than improvement, and parameter calibration may not rectify the issue.

426 The results of the P+ICE scenario (Figure 2 a-c), which considered both soil ice
427 effects in the SMP scheme, showed improvements in soil temperature simulation at any
428 depth when compared to the other schemes, as demonstrated by the generally higher
429 mean, median and IQR values of NSE. The performance of P+ICE in soil moisture
430 simulation was more complicated. The P+ICE scheme showed similar accuracy to the
431 Baseline and higher accuracy than P and ICE at 2.45 m depth (Figure 2 f), and the best
432 accuracy of all schemes at 0.4 m depth (Figure 2 e). For the soil moisture simulation at
433 near-surface depth (0.05 m), although the mean and median values and the IQR of the
434 NSE in the P+ICE scenario were not as high as those of the Baseline, the minimum
435 NSE value in P+ICE was, in contrast, higher (Figure 1 d), indicating that the P+ICE
436 scheme has the advantage of preventing extremely poor soil moisture results at this
437 depth. Overall, this straightforward comparison across schemes based on ensemble
438 results demonstrates the importance of fully considering the physical effects of soil pore
439 ice on the SMP in simulations of soil freezing/thawing processes when parametric
440 uncertainties are netted out.

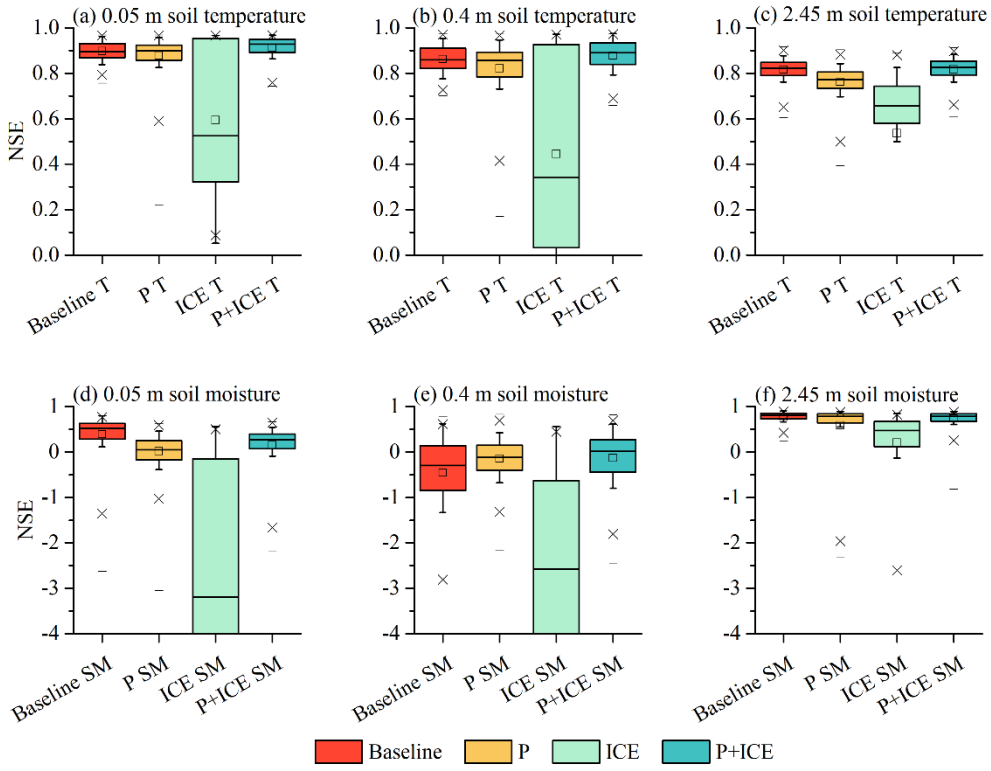

Figure 2 Boxplots showing the distributions of Nash-Sutcliffe Efficiency (NSE) values for four scenarios using different SMP schemes in the SHAW model to simulate soil temperature (T, a-c) and moisture (SM, d-f) at depths of 0.05 (a, d), 0.4 (b, e) and 2.45 (c, f) m at the TGL. The boxes depict the interquartile range (IQR) between the first quartile (Q1) and the third quartile (Q3), the horizontal line within the box represents the median, and the whiskers indicate the range from (Q1−1.5IQR) to (Q3+1.5IQR). The square symbol represents the mean value, the cross symbol represents the 1st and 99th percentile range, and the dash symbol represents the maximum and minimum values. Outliers are values outside of the whisker range. Extremely low NSE values in the ICE scenario have been excluded from the figures to improve readability.

3.2 Soil temperature and moisture content simulations

Figures 3 and 4 show the 95PPU bands for the uncertainties associated with the simulated soil temperature and moisture, respectively, based on ensemble runs of the four scenarios with different SMP schemes. The thicknesses of the 95PPUs for soil temperature and moisture in all scenarios are generally wider at the shallow (0.05 m, first columns in Figures 3 and 4) and intermediate depths (0.4m, second columns in Figures 3 and 4) than at deep depth (2.45 m, third columns in Figures 3 and 4). This is because heat and water migration near the bottom of the active layer is strongly controlled by the relatively stable underlying permafrost. The 95PPU bands of the simulated soil temperature for most scenarios show similar widths at all depths and well

capture the observed soil temperatures. However, the ICE scenario has a much greater thickness in bands, and the simulated means, especially at the shallow and intermediate depths (Figure 3g, h), exhibit inconsistency with the observations. By contrast, the 95PPU bands of the simulated soil moisture show significant differences among the SMP scenarios, with the ICE scenario being the worst at all depths (Figure 4g-i). These results demonstrate that the different considerations of soil ice effects on the SMP in a physical model can substantially affect the model's simulations of hydrological dynamics of frozen ground.

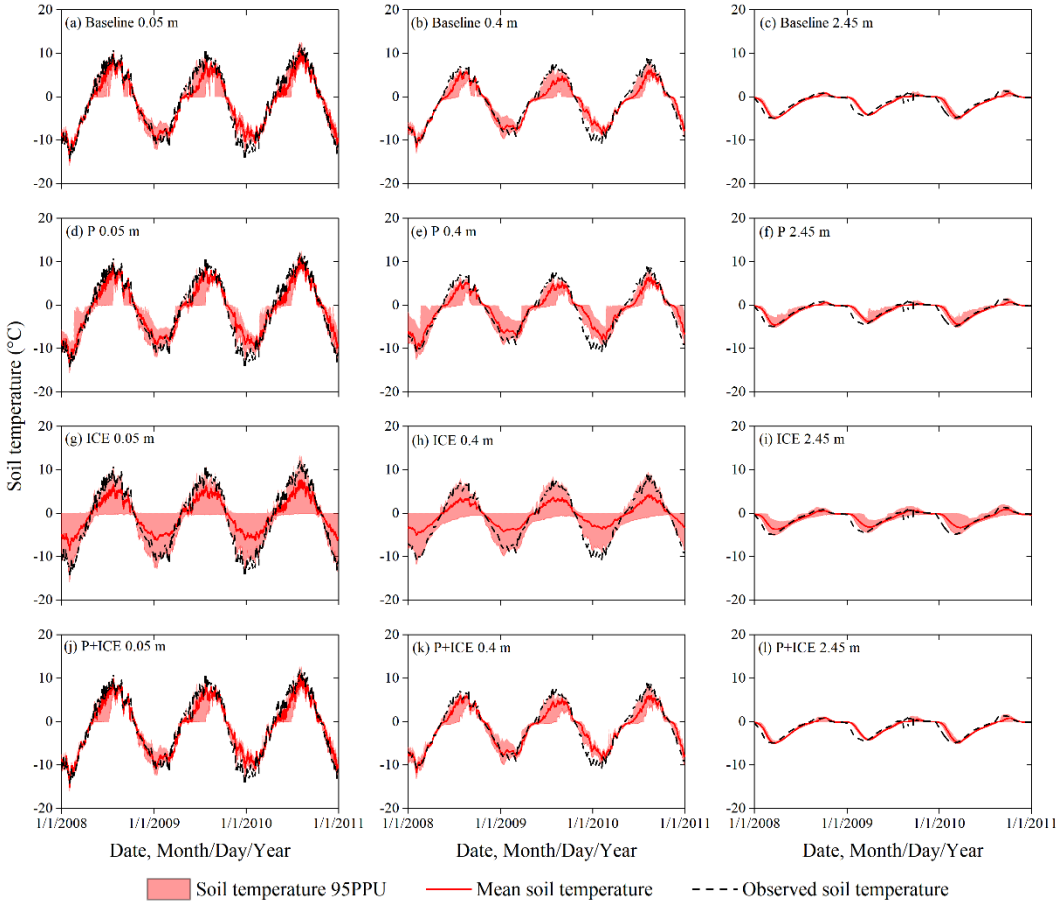

Figure 3 95 percent prediction uncertainty (95PPU) bands (red shaded areas) for simulated soil temperature at 0.05 m (left column), 0.40 m (mid column) and 2.45 m (right column) depths in different SMP scenarios. The red solid lines show the means of the soil temperature simulations based on all valid simulations of each SMP scenario. A valid simulation for an SMP scenario is one that runs for the entire simulation period (including spin-up period) without interruptions due to numerical non-convergence and corresponds to a certain combination of SMP-related parameter values randomly generated within preset ranges.

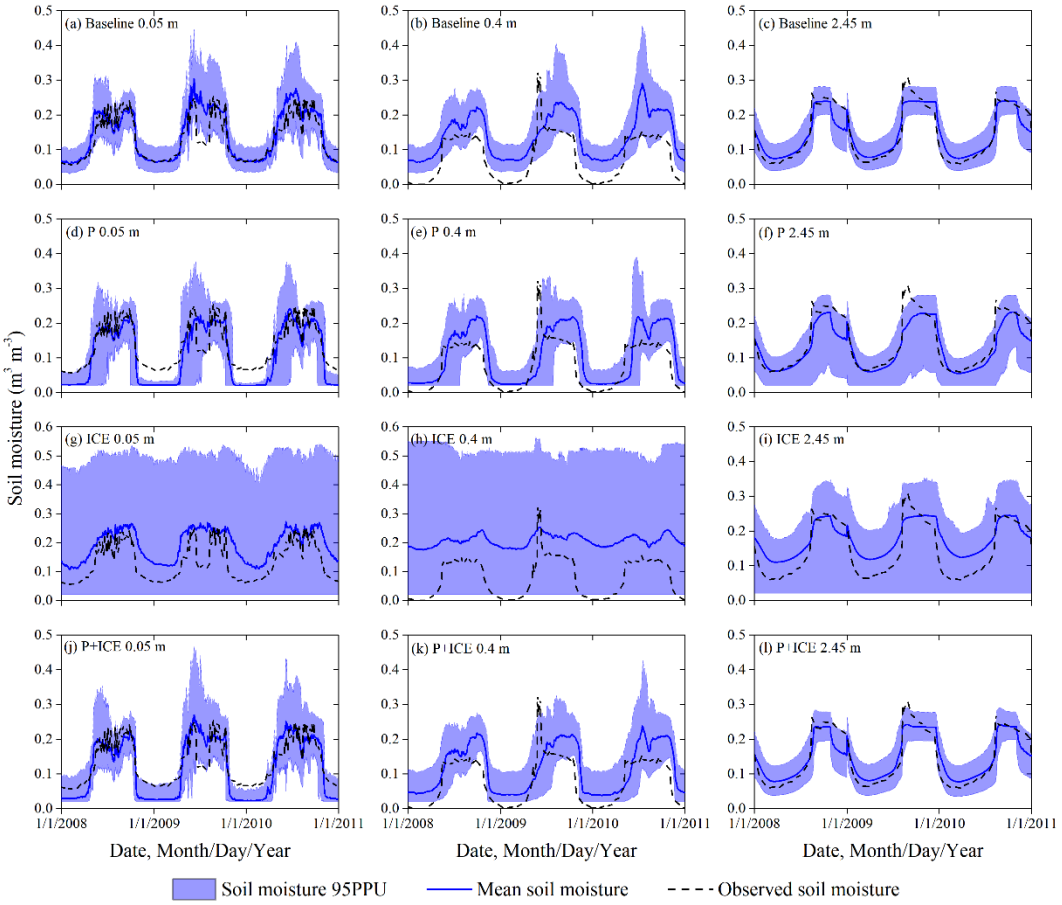

Figure 4 95PPU bands (blue shaded areas) for simulated soil moisture content at 0.05 m (left column), 0.40 m (mid column) and 2.45 m (right column) depths in different SMP scenarios. The same notations as in Figure 3 are applied.

The 95PPUs of the Baseline simulations can largely bracket the in-situ observations of soil temperature (Figure 3a-c) and moisture (Figure 4a-c), with mean values that agree well with the observations at almost all depths. This confirms a generally satisfactory accuracy of the original Campbell SMP method without ice's effects. However, the Baseline simulations exhibit a discrepancy with the observations for soil moisture content at 0.4 m depth, where the simulations overestimate the soil moisture content during frozen periods (Figure 4b). Additionally, the Baseline simulations of soil temperature exhibit thick 95PPU bands during spring thaw and fall freeze periods at 0.05 m and 0.4 m depths, which entail a risk of significant biases due to parameter uncertainties (Figure 3a-b).

The simulations of both soil temperature and moisture for the P and ICE scenarios, which consider only a partial effect of soil ice on the SMP, show substantial differences in 95PPUs from those of the Baseline. The UWC simulated in P dropped to very low levels during frozen periods (Figure 4d-e) at depths of 0.05 and 0.4 m as a result of a reduced effective porosity as pore ice grew. This leads to large negative

biases at 0.05 m when compared to the observations (Figure 4d). However, these low simulated UWC values agree well with observations at 0.4 m depth due to the extremely low observed values at this depth (Figure 4e). Consequently, the unsatisfactory accuracy of unfrozen water simulation in the P scenario undermined the simulation of heat transport, resulting in wider 95PPU bands for soil temperature in freeze periods (Figure 3d-f).

The 95PPU bands of soil moisture for the ICE scenario display excessive thickness at all three selected depths (Figure 4g-i), suggesting that most valid simulations face challenges reproducing the observations solely based on the cryosuction effect considered in the SMP scheme. The mean simulated soil moisture time series were also substantially overestimated in comparison to the observations. The soil moisture simulations of the ICE exhibited poor performance not only in the freeze periods but also in the thaw periods, owing to the propagation of large errors that occur in the freeze periods to later periods. Zheng et al. (2017) also reported an overestimation of UWC, suggesting that the inclusion of only the effect of cryosuction in the SMP parameterization with a C_k of 8 can multiply the content of residual unfrozen water during freezing periods. This causes water to flow from unfrozen layers to the freezing fronts during the freezing process, eventually leading to an oversaturated water equivalent at some specific layers. Since the model tightly couples heat and water processes, it is not surprising that the ICE scenario produced a narrower annual oscillation of soil temperature than those observed at all depths and wider 95PPU spreads than other scenarios (Figure 3g-i). The overall unsatisfactory performance of the ICE scenario implies that the SMP scheme, which considers only the effect of cryosuction in model, is unsuitable for simulating the freezing-thawing processes in cold regions.

The P+ICE scenario, which incorporates both soil ice effects on the SMP, outperformed the P and ICE scenarios, which only partially accounted for soil ice effects, in both soil moisture and temperature simulations. Throughout the simulation period, discrepancies between the P+ICE and Baseline simulations were minor, with the exception of freeze periods. As shown in Figure 4b, e, h, and k, UWC at the intermediate depth (0.4 m) was consistently observed to be significantly lower than at other depths during freezing periods. The ensemble simulations of P+ICE more accurately captured this lower UWC at 0.4 m depth than those of Baseline. At 0.05 m, the P+ICE simulations still slightly underestimated UWC during frozen periods compared to observations (Figure 4j), indicating accounting for cryosuction alone is not sufficient to fully correct for the underestimations caused by effective porosity. However, the P+ICE bands could still broadly bracket observed soil moisture contents at 0.05 m depth, suggesting that this underestimation can be mitigated through careful parametric calibration. In contrast, all valid P simulations exhibited soil moisture contents that were consistently lower than observations during frozen periods at 0.05 m (Figure 4d), making parameter calibration ineffective in compensating for the

discrepancy. Moreover, compared to those of Baseline, the P+ICE scenario had smaller uncertainties in soil temperature simulations at 0.05 m and 0.4 m during the autumn freeze, as evidenced by the much thinner 95PPU of the soil temperature during these periods (Figure 3a, b and j, k). This indicates the inclusion of both soil ice effects in the SMP scheme can effectively improve soil temperature simulations during phase change processes.

3.3 Parameter identifiability and optimal parameter space

Figure 5 shows the relationship between soil temperature NSE and saturated vertical conductivity, $\boldsymbol{K_s}$, based on valid simulations using randomly generated values for the four SMP-related parameters, under the four SMP scenarios, while Figure 6 presents the corresponding results for soil moisture simulations. The corresponding probability densities of $\boldsymbol{K_s}$ at the 0.05 m depth are also provided in the figures. We found that for all scenarios, higher NSEs of soil temperature simulations at depths of 0.05 and 0.4 m were achieved when relatively lower $\boldsymbol{K_s}$ values of less than 20 $cm \cdot h^{-1}$ were used(Figure 5a-h). Futhermore, we observed that a higher NSE associated with a $\boldsymbol{K_s}$ value less than 20 $cm \cdot h^{-1}$ consistently yielded a better simulation of soil temperature, regardless of other parameters. We confirmed the characteristic of a low $\boldsymbol{K_s}$ being preferable by examining the distributions of the other parameters at a $\boldsymbol{K_s}$ less than 20 $cm \cdot h^{-1}$, as expected by the nature of Latin hypercube sampling, where each parameter is independently and uniformly sampled (Loh, 1996).

In contrast, a greater $\boldsymbol{K_s}$ gave a better simulation of soil temperature at the bottom (2.45 m) depth for the Baseline, P and P+ICE scenarios, with an exception for the ICE scenario where a small $\boldsymbol{K_s}$ remained preferable. While the probability density of $\boldsymbol{K_s}$ should uniformly distribute over the predetermined range, $\boldsymbol{K_s}$ values from the valid simulations of the scenarios with cryosuction considered (ICE and P+ICE) remained only small (Figure 5o and p). This indicates that numerical instability due to cryosuction can be prevented by a lower $\boldsymbol{K_s}$. A similar relationship was also found for soil moisture simulations, suggesting that a lower $\boldsymbol{K_s}$ is conducive to achieve accurate soil moisture simulation at the shallow depths of the active layer. However, $\boldsymbol{K_s}$ is less likely to affect the soil moisture simulation at 2.45 m depth, where soil migration infrequently occurs during a year.

In addition to $\boldsymbol{K_s}$, the saturated water content, $\boldsymbol{\theta_s}$, also controls liquid water movement through the soil by serving as a key parameter in Richards' equation. Compared to soil temperature (Figure 7), the accuracy of soil moisture simulations is more strongly regulated by $\boldsymbol{\theta_s}$, as shown in Figure 8. However, the optimal space for $\boldsymbol{\theta_s}$ varied significantly among SMP schemes. For the Baseline and P+ICE, a $\boldsymbol{\theta_s}$ value in an interval of 0.35 to 0.40 $m^3 \cdot m^{-3}$ yielded the best performance of soil moisture simulation at depths of 0.05 and 2.45 m (Figure 8a, d, i and l). For the remaining selected depth (0.4 m) where the observed soil moisture content was relatively low, a lower $\boldsymbol{\theta_s}$ of about 0.3-0.35 $m^3 \cdot m^{-3}$ was necessary for the best fit in the Baseline and

P+ICE (Figure 8e and h). In contrast, in the P scenario, where the residual UWC was systematically underestimated during frozen seasons, a higher $\boldsymbol{\theta_s}$ between 0.5 to 0.6 $m^3 \cdot m^{-3}$ was needed; otherwise, the UWC would be similarly negatively biased (Figure 8b, f and j). The ICE scheme did not demonstrate an optimal range for $\boldsymbol{\theta_s}$ at any soil depth, but maintaining a relatively higher $\boldsymbol{\theta_s}$ above 0.4 $m^3 \cdot m^{-3}$ could be beneficial in reducing potential computational errors, such as the range of 0.4 $m^3 \cdot m^{-3}$ to 0.6 $m^3 \cdot m^{-3}$ with a high probability density of $\boldsymbol{\theta_s}$ (Figure 7o).

No specific optimal intervals were identified for the air entry potential ($\boldsymbol{\psi_e}$) and pore size distribution ($\boldsymbol{b}$) parameters that would significantly improve the accuracy of soil temperature and moisture simulations (Figures S1-4). While simulations with a high $\boldsymbol{\psi_e}$ at depths of 0.05 and 0.4 m and a low $\boldsymbol{\psi_e}$ at a depth of 2.45 m probably exhibited slightly better accuracy, it showed that these parameters do not have optimal solutions and are not as behavioral as $\boldsymbol{K_s}$ and $\boldsymbol{\theta_s}$ in controlling heat and water fluxes within the active layer in our experiment.

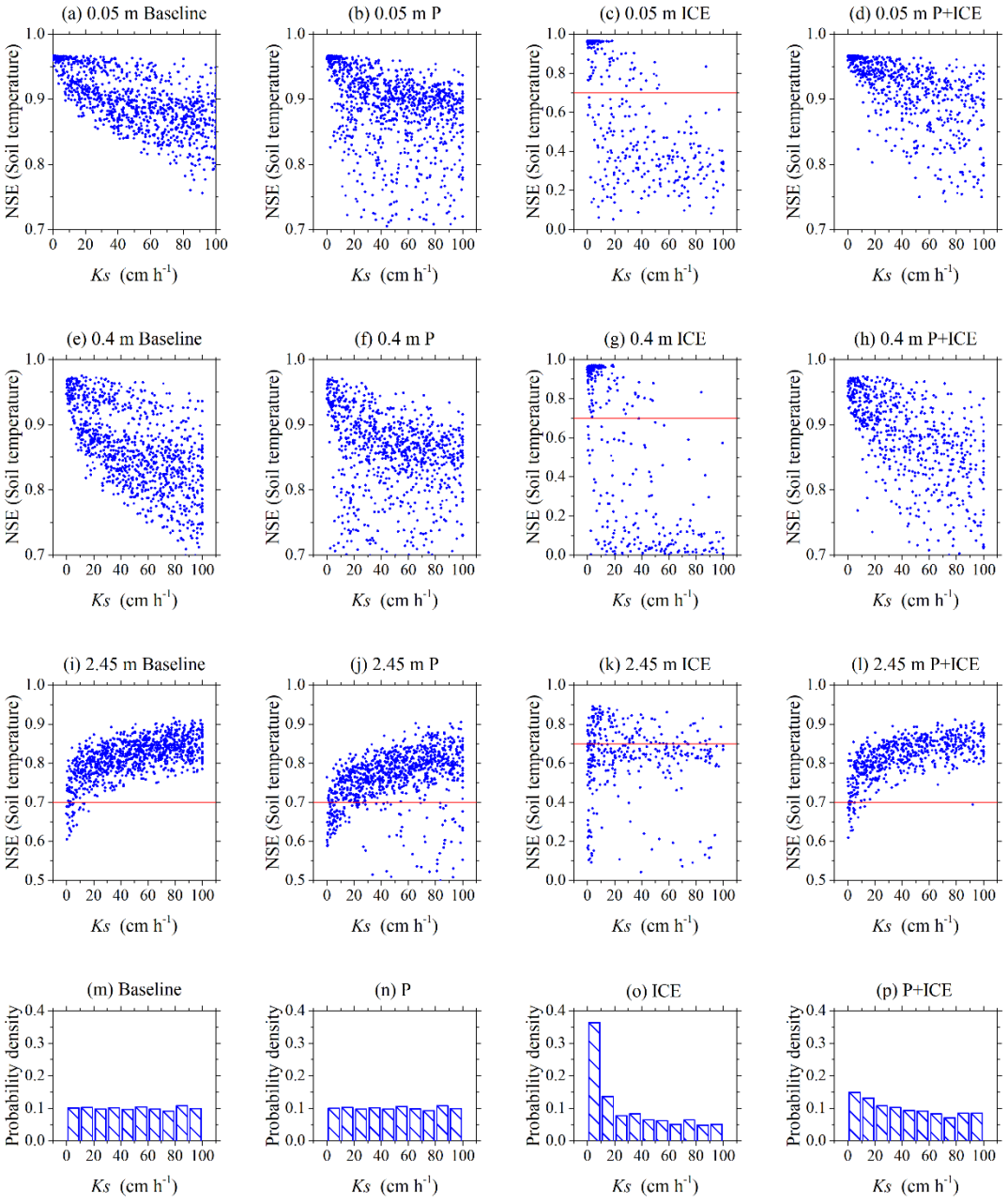

Figure 5 Scatter plots showing the distribution patterns of NSE versus saturated vertical conductivity (K_s) based on valid soil temperature simulations at depths of 0.05 m (a-d), 0.4 m (e-h) and 2.45 m (i-l) for the four scenarios with different SMP schemes in the SHAW model. The probability density distribution of K_s for the 0.05 m depth sampled using the Latin hypercube sampling method is shown for each scenario (m-p). Other depths have similar K_s sampling distributions and are therefore not shown. The red horizontal lines indicate an NSE value of 0.7, which represents a satisfactory level of simulation accuracy for soil temperature.

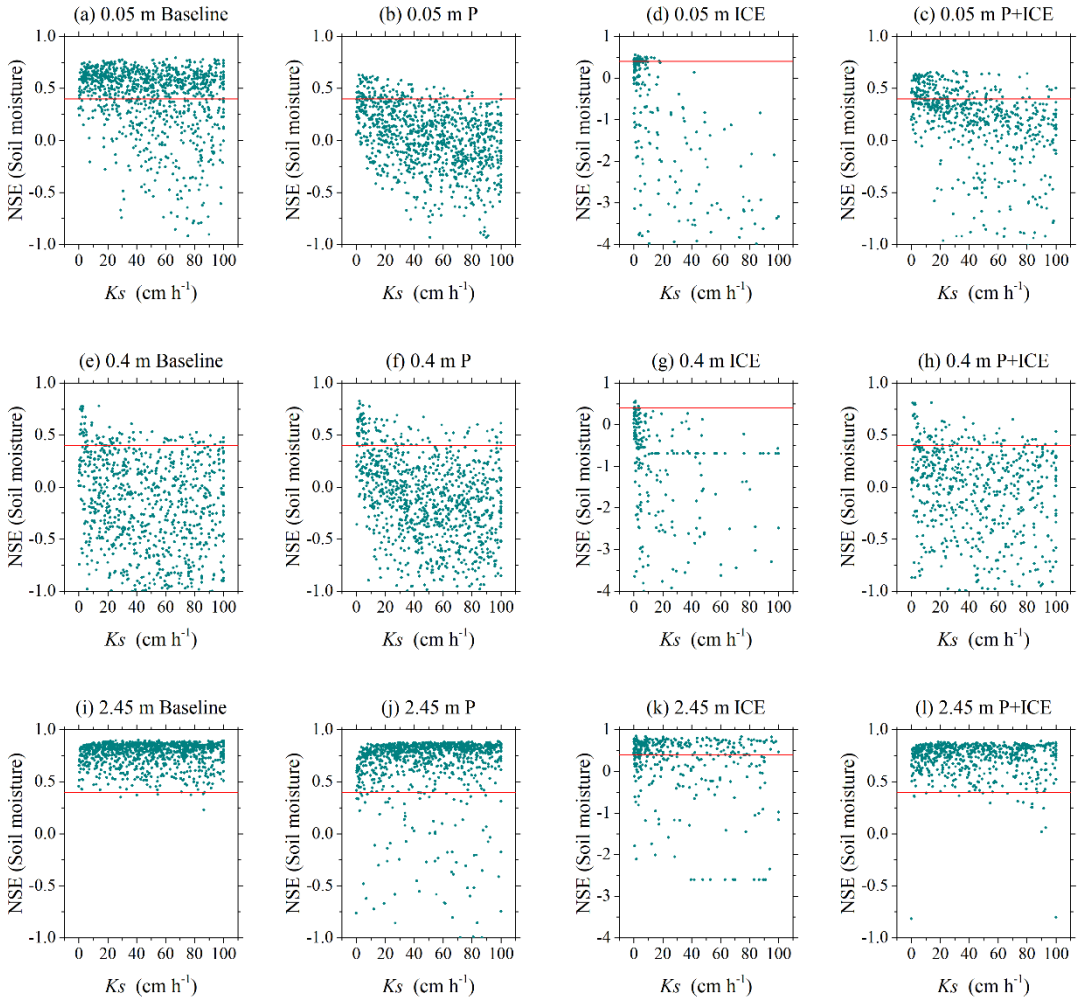

Figure 6 Scatter plots showing the distribution patterns of NSE versus saturated vertical conductivity (K_s) based on valid soil moisture simulations at depths of 0.05 m (a-d), 0.4 m (e-h) and 2.45 m (i-l) for the four scenarios with different SMP schemes in the SHAW model. The probability density distributions of K_s are the same as those shown in Figure 5. The red horizontal lines indicate an NSE value of 0.4, which represents a satisfactory level of simulation accuracy for soil moisture.

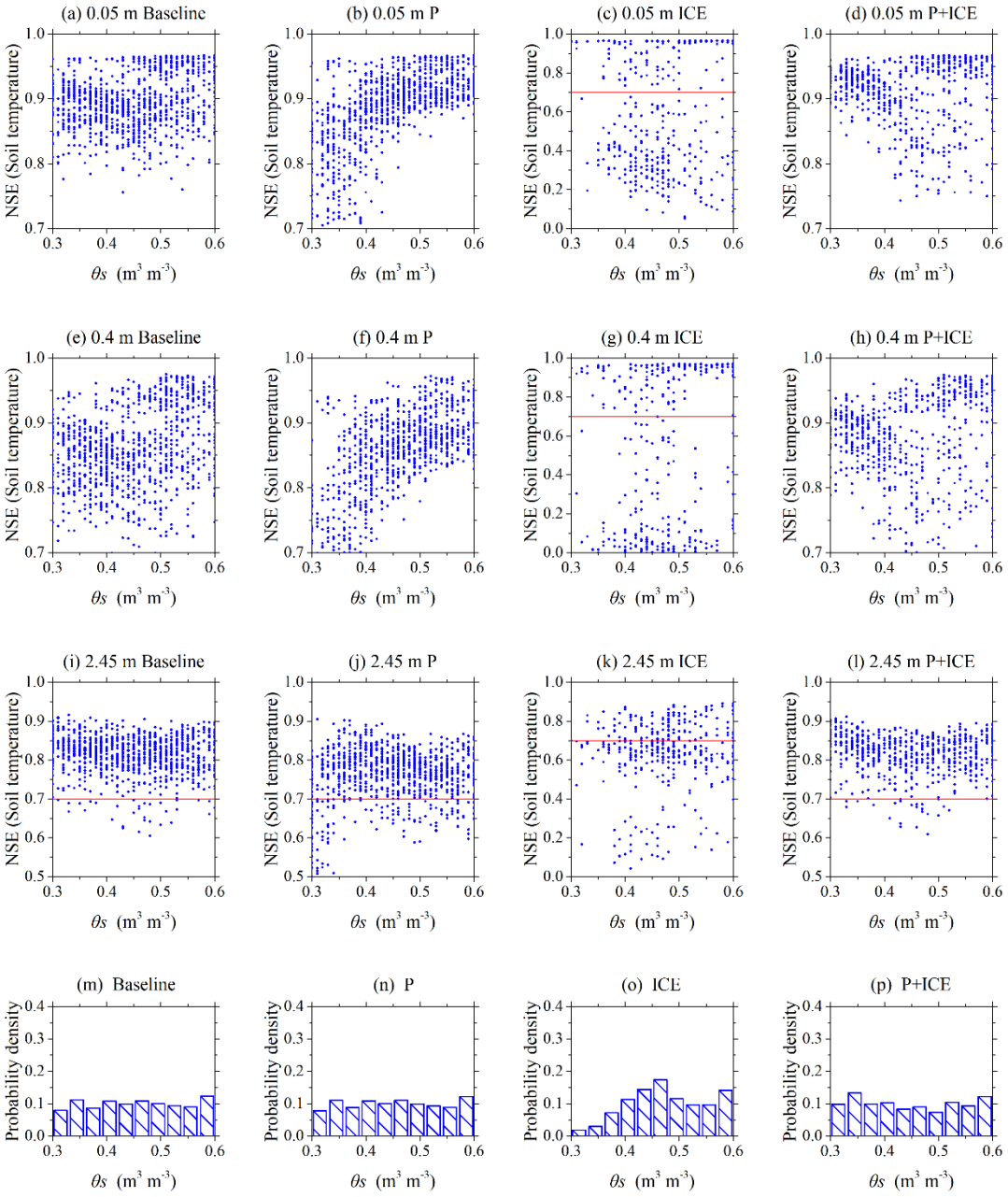

Figure 7 Scatter plots showing the distribution patterns of NSE versus saturated water content (θ_s) based on valid soil temperature simulations at depths of 0.05 m (a-d), 0.4 m (e-h) and 2.45 m (i-l) for the four scenarios with different SMP schemes in the SHAW model. The probability density distribution of θ_s for the 0.05 m depth sampled by the Latin hypercube sampling method is shown for each scenario (m-p). Other depths have similar θ_s sampling distributions and are therefore not shown. The red horizontal lines indicate an NSE value of 0.7, which represents a satisfactory level of simulation accuracy for soil temperature.

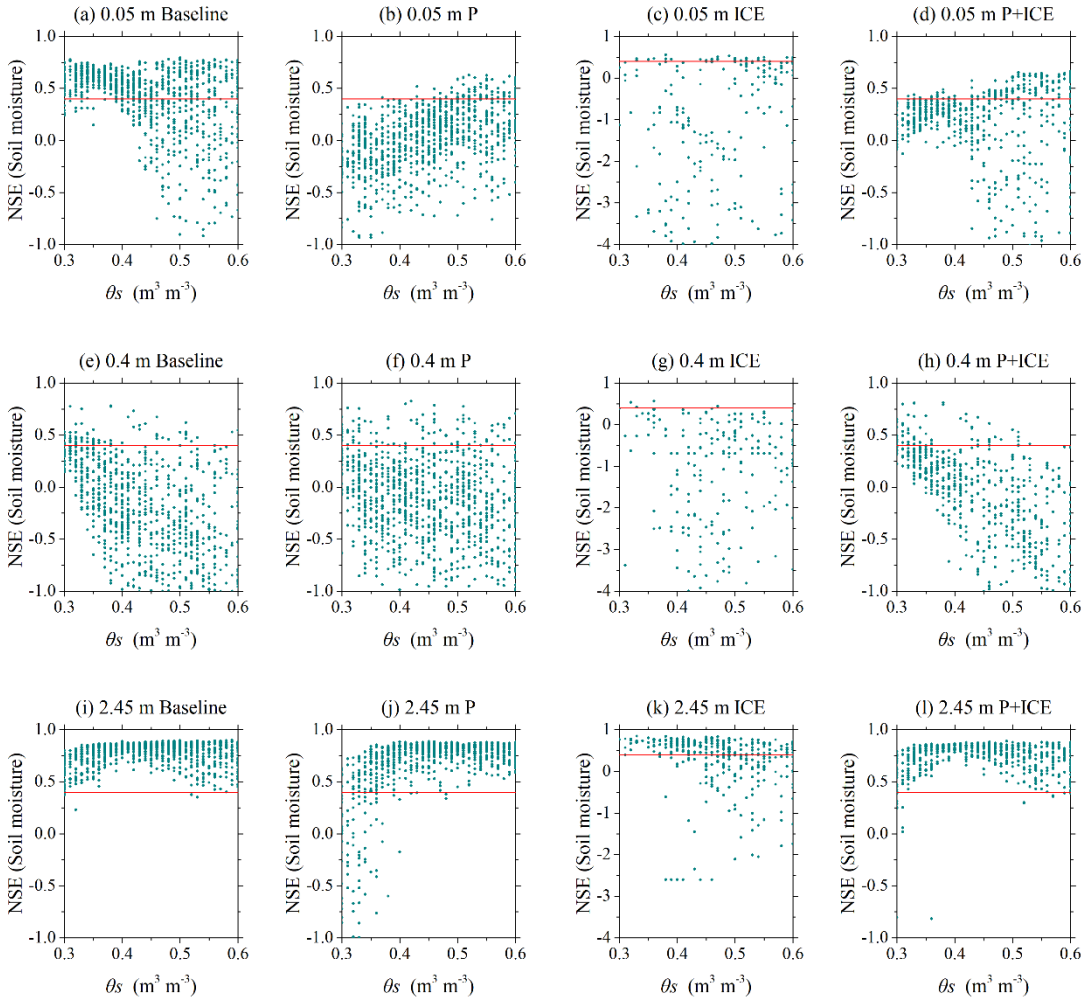

Figure 8 Scatter plots showing the distribution patterns of NSE versus saturated water content (θ_s) based on valid soil moisture simulations at depths of 0.05 m (a-d), 0.4 m (e-h) and 2.45 m (i-l) for the four scenarios with different SMP schemes in the SHAW model. The probability density distributions of θ_s are the same as those shown in Figure 7. The red horizontal lines indicate an NSE value of 0.4, which represents a satisfactory level of simulation accuracy for soil moisture.

4 Discussion

4.1 Importance of soil pore ice representation in SMP parameterizations

Cryosuction causes the redistribution of liquid water within the active layer by increasing the soil potential at the top-down and bottom-up freezing fronts and migrating the liquid water from the unfrozen layer to freezing fronts. While there is no consensus on the optimal representation of cryosuction in the SMP equation, previous studies have extensively tested and verified the effectiveness of a modified Campbell-based scheme proposed by Kulik (1978), which includes an additional term to account for cryosuction (Eq.3), in simulating hydrological processes in frozen soils (Koren et al., 1999; Li et al., 2010; Wang et al., 2017; Wang et al., 2021; Zhang et al., 2007).

636 However, our experiment and several previous studies (Stuurop et al., 2021; Zheng et
637 al., 2017) have shown that this approach often leads to poor simulations due to
638 overestimation of UWC and consequent biases in soil temperature simulation. This
639 apparent contradiction could be explained by the fact that most relevant studies rely on
640 precisely calibrated parameter values, which can compensate for the physical
641 shortcomings of such a scheme. In contrast, our findings are derived from an ensemble
642 simulation of the SHAW model using randomly generated SMP-related parameter sets.
643 Therefore, the cryosuction-only form of the SMP scheme is not recommended for use
644 in applications in cold regions, especially where there is insufficient data for parameter
645 calibration.

646 The effective porosity of the soil changes dynamically with the accretion of soil
647 ice and exerts an important influence on the SMP of frozen soils. As ice gradually fills
648 soil pores, the pore space available for water migration decreases. Our study, as well as
649 Xiao et al.(2013), which evaluated the CoLM hydraulic parameterization scheme that
650 incorporates the effect of effective porosity, found that the SMP scheme that considers
651 only the effective porosity (Eq.2) resulted in an extremely low residual UWC during
652 the freezing seasons (Figure 4d, e and f). This may compromise the simulation of soil
653 temperature, as more soil pore ice increases both heat conduction and latent heat. Both
654 theoretical analyses and numerical simulations suggest that considering the effect of
655 either cryosuction or effective porosity alone in an SMP scheme negatively affects the
656 model performance when simulating hydrological and thermal dynamics in permafrost
657 regions.

658 As demonstrated in this study, the opposing effects of cryosuction and effective
659 porosity on UWC can offset each other when both are present. This explains why the
660 Baseline scenario, which ignores both effects, can still achieve decent simulation
661 accuracy. However, it is important to note that the Baseline still has physical limitations
662 and is weak in accurately representing the complex hydrological and thermal processes
663 of frozen soil. This includes overestimation of UWC in the mid-depth of active layer
664 and large uncertainties in simulating soil temperature during freezing and thawing
665 periods.

666 An SMP scheme considering both soil ice effects, i.e., the P+ICE scheme, is
667 able to overcome the weaknesses of the P and ICE schemes and provide improved
668 simulation accuracy for both soil temperature and moisture. The P+ICE scheme
669 produced slightly higher NSEs for temperature simulations and 0.4 m soil moisture
670 simulations compared to the Baseline scenario, but its strength lies in its more accurate
671 representation of the physical processes involved. By accounting for the role of ice in
672 the soil potential, the P+ICE simulation successfully reproduces the soil water
673 redistribution within the active layer due to cryosuction at the freezing fronts and
674 accurately simulates the extremely low residual UWC at the intermediate depth of the
675 active layer (Figure 4k). However, P+ICE still slightly underestimates the UWC at 0.05
676 m, likely due to the mathematical nature of considering effective porosity, suggesting

that careful parameter calibration is still necessary. Because heat transfer, phase change and the presence of ice are strongly coupled in frozen soils, the improved representation of pore ice in the SMP, as demonstrated, helps to improve the soil temperature simulation during the freezing process (Figure 3j, k). However, such significant improvement in temperature simulation is not observed in the thawing process, as the impacts of ice gradually weaken during the transition from ice to liquid. Therefore, we advocate for the integration of an SMP scheme fully considering soil pore ice effects in an LSM for frozen ground applications, not only to improve the model's ability to simulate thermal and hydrological dynamics but also to accurately represent the freezing processes within the active layer.

4.2 Implications for SMP-related parameter identifiability

To avoid biased evaluation based on a single parameter set, we employed a random sampling method to explore the full parameter space of SMP-related parameters and investigated the responses of SMP schemes across the entire spaces. This approach is necessary for a thorough understanding of the performance of the SMP schemes and can provide guidance for parameter calibration. While it is important to note that not all randomly sampled parameter combinations are realistic in the natural environment, exploring the full parameter space can still provide valuable insights into the sensitivity of the SMP scheme to different parameters and help identify which parameters are most important for model performance. Furthermore, even if the optimal range for a certain parameter may fall outside the realistic range, understanding its impact can still be useful for evaluating the behavior of the SMP scheme and making informed decisions about selection and improvement of SMP schemes.

The saturated vertical hydraulic conductivity has great explanatory power for the performance of all SMP schemes by controlling the liquid flux migration within soil layers, even though it is not a direct component of the SMP equations. As freezing progresses, the soil ice grows in the pores and narrows liquid flow paths, thus blocking water fluxes in frozen soils (Chen et al., 2021). Our study found that all four SMP schemes recommend a relatively low saturated vertical conductivity, reflecting the dwindling permeability of frozen soils (Figures 5 and 6). Specifically, for the cryosuction-only scheme, a low saturated vertical conductivity helps offset overestimated UWC and water flow, ultimately reducing numerical instability. Some previous studies have used unrealistically low values of saturated vertical conductivity to improve simulation accuracy in models that apply an SMP parameterization solely based on the cryosuction effect (Stuurop et al., 2021; Zhang et al., 2007).

The saturated water content defines the maximum water content that a soil layer can contain and directly affects soil migration and distribution in the SHAW model. Unlike saturated vertical hydraulic conductivity, the saturated water content is typically determined by soil physical properties and allows for limited calibration. A suitable value for saturated water content depends on soil texture and hydraulic characteristics

717 in the study area and the SMP scheme used in the model. In our experiment, a saturated
718 water content value between 0.3 to 0.4 $m^3 \cdot m^{-3}$ is preferable for the Baseline and P+ICE
719 simulations. However, a higher value may be needed for the P and ICE scenarios to
720 compensate for their limitations in physical representation. While it may be
721 mathematically effective, we caution against using excessively high values that are
722 unrealistic in real-world settings. Rather, we encourage improving the physical
723 representation to ensure accuracy and reliability in simulations.

724 The empirical parameter, C_k, is a crucial factor that controls the cryosuction
725 magnitude. In our study, a value of 8 was used for ICE and P+ICE scenario, which is
726 widely applied in many studies (Koren et al., 1999; Wang et al., 2017; Wang et al.,
727 2021; Zhang et al., 2007) and suggested as an average value by Kulik (1978). However,
728 a large number of randomly generated parameter sets that were feasible for the original
729 Campbell method failed to converge numerically in the ICE-included scenarios. To
730 address this issue, some studies have suggested a value of C_k less than 3 for the
731 cryosuction-only SMP scheme (Ganji et al., 2017; Stuurop et al., 2021; Zheng et al.,
732 2017). We tested a lower value of about 2 for C_k in the ICE scenario, which showed
733 improvement compared to C_k of 8 but was still inferior to the P+ICE scenario with a
734 C_k of 8 (Figures S5 and S6). Using a much low value of C_k to compensate for the lack
735 of effective porosity may result in overfitting and neglecting the physical process in the
736 model. Instead, we incorporated the effect of effective porosity into the same SMP
737 equation (Eq.4) to greatly alleviate the overestimation of UWC due to cryosuction, even
738 at a C_k of 8.

739 4.3 Limitations

740 This study has some limitations that should be acknowledged. While we focused
741 on SMP parameterizations based on the Campbell equation, it is worth noting that there
742 are other SMP equations in different forms, such as the Brooks-Corey equation (Brooks,
743 1964) and van Genuchten equation (van Genuchten, 1980), wich are also widely used
744 in cold region studies (Cheng et al., 2015; Lv et al., 2021; Pan et al., 2019). One
745 significant difference between these equations and the Campbell equation is that they
746 consider residual UWC (Eq. 11), which is not explicitly considered in the Campbell
747 equation:

748 $$S = \frac{\theta_l - \theta_r}{\theta_s - \theta_r} \quad (11)$$

749 where S is the normalized soil wetness and θ_r is the residual water content based on an
750 assumption that liquid flow processes are negligible when θ_l is less than θ_r. Since there
751 is still no conclusive experimental evidence that a θ_r exists in nature conditions
752 (Nimmo, 1991), θ_r is usually treated as a fitted parameter in most studies, which can
753 lead to unrealistic or even negative values (Groenevelt & Grant, 2004). In our study,
754 we did not consider θ_r in our schemes due to the wide difference in UWC between
755 shallow and mid-depth active layers, as shown by the observed soil moisture content at

the TGL (Figure 4). This makes it difficult to propose a specific θ_r for the entire soil column, which could introduce unnecessary uncertainties. However, our findings can still provide insights for other SMP equations such as the Brooks-Corey and van Genuchten equations, which are based on the same theoretical basis as the Campbell equation. This theoretical basis determines the SMP based on the relative soil wetness estimated from liquid water content and soil porosity, similar to the Campbell equation.

The accuracy of the simulations is greatly impacted by uncertainties associated with input meteorological data and field observations. The harsh physical environment on the QTP has resulted in a lack of long-term, high-quality in-situ climate and permafrost observations, which is a major obstacle. The TGL site is the only site that can provide quality observations of both long-term forcing and active layer dynamics to support the SHAW simulations. Consequently, we have limited opportunities to verify the same SMP scenarios elsewhere on the QTP with differential land surface and soil texture conditions, which can affect heat and water transfer within the soil (Harp et al., 2016; Wang et al., 2019). Nonetheless, this study thoroughly examined SMP-related soil hydraulic parameters that are highly related to soil texture and their impact on frozen soil thermal and hydrological dynamics. Thus, the findings may partially reflect the influence of soil texture on frozen soil hydrology.

Additionally, other factors osmotic potential caused by soil solution (Harrysson Drotz et al., 2009) and rheological or Van der Waals force (Fisher et al., 2020) have been reported to affect soil hydrology in frozen ground. While we conducted a preliminary examination of the contribution of solutes to soil temperature and hydrology simulations using sample data from the official SHAW site (USDA, 2019), we found that the difference in output model variables caused by considering solutes was minimal. However, due to the lack of necessary data on the TGL site and model representations, these factors were excluded from the SHAW model in this study.

5 Conclusions

This study evaluated four frozen soil SMP parameterization schemes that represent the effects of soil pore ice in different ways. The four schemes included one that completely ignores the effects of soil ice, two that partly consider the effects of soil ice (i.e., effective porosity or cryosuction), and a newly proposed scheme that considers both effective porosity and cryosuction. The evaluation was conducted within the same SHAW model, using the same forcing data from the TGL permafrost site, and based on an ensemble run with 1000 randomly generated combinations of SMP-related parameters to facilitate uncertainty analysis.

Our results showed the SMP schemes with partial inclusion of soil ice effects led to great biases in the model simulation, negatively affecting the model performance. Specially, the scheme that only considers the effect of effective porosity seriously underestimated UWC during the freeze periods, while the scheme that only considers the effect of cryosuction overestimated UWC. These poor simulations of UWC by these

two schemes resulted in great biases in simulating both heat and water dynamics of frozen soil, greatly hampering their applications in cold regions.

Due to the oppositing effects of effective porosity and cryosuction on the SMP, the SMP scheme without either of them may still produce acceptable simulations of the heat and water dynamics of the active layer, but still has uncertainties in simulating temperatures at shallow and intermediate depths during the water phase change periods. This indicates that the absence of physical representations for soil ice can still lead to problematic simulations.

The full SMP scheme, which accounts for the effects of both effective porosity and cryosuction, has the highest accuracy in simulating frozen soil temperature and significantly reduces the biases that occur with the two schemes that only partly considered the effects. Compared to the scheme without soil ice, the full consideration of soil ice in this scheme improves the simulation of the liquid-to-ice process by reducing the large uncertainties of temperature simulations during freeze periods. This scheme is also advantageous in simulating the relatively low residual UWC at the intermediate soil depth of the active layer. Overall, this study sheds light on the important of considering soil ice effects in frozen soil SMP parameterizations for accurate simulation of frozen soil hydrology. We recommend the full SMP scheme to be incorporated in current LSMs for applications in cold regions.

This study also provides insights for the application of these schemes from the perspective of the parameters involved. A lower saturated vertical hydraulic conductivity, which reflects the reduction in soil permeability, is advised for all four scenarios to obtain good simulations and mitigate potential numerical instability when cryosuction is included in the SMP scheme. A particularly high saturated water content is necessary for the scheme only considering effective porosity to compensate for the underestimation of UWC during freeze periods, although such a high value of saturated water content rarely occurs in the real world. These findings can help guide the selection and parameterization of SMP schemes in future studies of frozen soil.

Code and data availability

The source codes of the Simultaneous Heat and Water (SHAW) model are available on the USDA Agricultural Research Service website (https://www.ars.usda.gov/pacific-west-area/boise-id/northwest-watershed-research-center/docs/shaw-model/, accessed September 4, 2022). The modified codes and simulation results of this study are publicly available at https://doi.org/10.6084/m9.figshare.20884237. The meteorological forcing data and measured temperature and moisture data of the active layer at the Tanggula site being studied can be downloaded from National Tibetan Plateau Data Center at https://doi.org/10.11888/Geocry.tpdc.271107 (accessed September 4, 2022).

Author contributions

YZ and ZN conceived and conceptualized the idea; YZ and ZN developed the methodology; YZ, HJ and ZC performed the analyses; ZN acquired the funding and provided the resources; ZN supervised the study; YZ wrote the draft version; and ZN, YZ and JH reviewed and edited the writing.

Declaration of interests

The contact author has declared that neither they nor their co-authors have any competing interests.

Acknowledgments

This work was supported by the Second Tibetan Plateau Scientific Expedition and Research (STEP) program (grant no. 2019QZKK0905-5) and the National Natural Science Foundation of China (grant nos. 42171125 and 41971074). The authors thank the National Tibetan Plateau Data Center for providing data and the USDA Agricultural Research Service for providing the model.

References

Akyurt, M., Zaki, G., Habeebullah, B. (2002). Freezing phenomena in ice-water systems. *Energy Conversion and Management, 43*(14), 1773-1789. https://doi.org/10.1016/s0196-8904(01)00129-7

Andresen, C. G., Lawrence, D. M., Wilson, C. J., McGuire, A. D., Koven, C., Schaefer, K., et al. (2020). Soil moisture and hydrology projections of the permafrost region – a model intercomparison. *The Cryosphere, 14*(2), 445-459. https://doi.org/10.5194/tc-14-445-2020

Azmatch, T. F., Sego, D. C., Arenson, L. U., Biggar, K. W. (2012). New ice lens initiation condition for frost heave in fine-grained soils. *Cold Regions Science and Technology, 82*, 8-13. https://doi.org/10.1016/j.coldregions.2012.05.003

Beven, K. (2006). A manifesto for the equifinality thesis. *Journal of Hydrology, 320*(1-2), 18-36. https://doi.org/10.1016/j.jhydrol.2005.07.007

Blyth, E. M., Arora, V. K., Clark, D. B., Dadson, S. J., De Kauwe, M. G., Lawrence, D. M., et al. (2021). Advances in land surface modelling. *Current Climate Change Reports, 7*(2), 45-71. https://doi.org/10.1007/s40641-021-00171-5

Boike, J., Roth, K., Overduin, P. P. (1998). Thermal and hydrologic dynamics of the active layer at a continuous permafrost site (Taymyr Peninsula, Siberia). *Water Resources Research, 34*(3), 355-363. https://doi.org/10.1029/97WR03498

Brooks, R. H. (1964). *Hydraulic properties of porous media.*, Colorado State University, Colorado.

Campbell, G. S. (1974). A simple method for determining unsaturated conductivity from moisture retention data. *Soil science, 117*(6), 311-314.

Chen, J., Gao, X., Zheng, X., Miao, C., Zhang, Y., Du, Q., Xu, Y. (2019). Simulation of soil freezing and thawing for different groundwater table depths. *Vadose Zone Journal, 18*(1), 1-14. https://doi.org/10.2136/vzj2018.08.0157

Chen, J., Mei, S., Rempel, A. W. (2021). Estimating permeability of partially frozen soil using floating random walks. *Water Resources Research, 57*(12). https://doi.org/10.1029/2021WR030598

Cheng, D., Wang, Y., Duan, J., Chen, X., Yang, S. (2015). A new analytical expression for ultimate specific yield and shallow groundwater drainage. *Hydrological Processes, 29*(8), 1905-1911. https://doi.org/10.1002/hyp.10306

Cheng, G. (1983). The mechanism of repeated-segregation for the formation of thick layered ground ice. *Cold Regions Science and Technology, 8*(1), 57-66. https://doi.org/doi.org/10.1016/0165-232X(83)90017-4

Cui, L., Zhu, Y., Zhao, T., Ye, M., Yang, J., Wu, J. (2020). Evaluation of upward flow of groundwater to freezing soils and rational per-freezing water table depth in agricultural areas. *Journal of Hydrology, 585*, 124825. https://doi.org/10.1016/j.jhydrol.2020.124825

Dai, Y., Zeng, X., Dickinson, R. E. (2001). *Common Land Model (CLM) Technical documentation and user's guide*. Beijing.

Dai, Y., Zeng, X., Dickinson, R. E., Baker, I., Bonan, G. B., Bosilovich, M. G., et al. (2003). The Common Land Model. *Bulletin of the American Meteorological Society, 84*(8), 1013-1024. https://doi.org/10.1175/BAMS-84-8-1013

Dall'Amico, M., Endrizzi, S., Gruber, S., Rigon, R. (2011). A robust and energy-conserving model of freezing variably-saturated soil. *The Cryosphere, 5*(2), 469-484. https://doi.org/10.5194/tc-5-

469-2011

Fisher, D. A., Lacelle, D., Pollard, W. (2020). A model of unfrozen water content and its transport in icy permafrost soils: Effects on ground ice content and permafrost stability. *Permafrost and Periglacial Processes, 31*(1), 184-199. https://doi.org/10.1002/ppp.2031

Flerchinger, G. N. (1991). Sensitivity of soil freezing simulated by the SHAW model. *Transactions of the ASAE, 34*(6), 2381-2389. https://doi.org/10.13031/2013.31883

Flerchinger, G. N., Caldwell, T. G., Cho, J. (2012). Simultaneous Heat and Water (SHAW) Model: model use, calibration, and validation. *Transactions of the ASABE, 55*(4), 1395-1411. https://doi.org/10.13031/2013.42250

Flerchinger, G. N., Pierson, F. B. (1997). Modelling plant canopy effects on variability of soil temperature and water: model calibration and validation. *Journal of Arid Environments, 35*(4), 641-653. https://doi.org/10.1006/jare.1995.0167

Flerchinger, G. N., Saxton, K. E. (1989a). Simultaneous heat and water model of a freezing snow-residue-soil system I. Theory and development. *Transactions of the ASAE, 32*(2), 565-571. https://doi.org/10.13031/2013.31040

Flerchinger, G. N., Saxton, K. E. (1989b). Simultaneous heat and water model of a freezing snow-residue-soil system II. Field verification. *Transactions of the ASAE, 32*(2), 573-576. https://doi.org/10.13031/2013.31041

Ganji, A., Sushama, L., Verseghy, D., Harvey, R. (2017). On improving cold region hydrological processes in the Canadian Land Surface Scheme. *Theoretical and Applied Climatology, 127*(1-2), 45-59. https://doi.org/10.1007/s00704-015-1618-4

913 Groenevelt, P. H., Grant, C. D. (2004). A new model for the soil-water retention curve that solves the
914 problem of residual water contents. *European Journal of Soil Science, 55*(3), 479-485.
915 https://doi.org/10.1111/j.1365-2389.2004.00617.x
916 Guo, D., Wang, H. (2013). Simulation of permafrost and seasonally frozen ground conditions on the
917 Tibetan Plateau, 1981-2010. *Journal of Geophysical Research: Atmospheres, 118*(11), 5216-
918 5230. https://doi.org/10.1002/jgrd.50457
919 Harp, D. R., Atchley, A. L., Painter, S. L., Coon, E. T., Wilson, C. J., Romanovsky, V. E., Rowland, J.
920 C. (2016). Effect of soil property uncertainties on permafrost thaw projections: a calibration-
921 constrained analysis. *The Cryosphere, 10*(1), 341-358. https://doi.org/10.5194/tc-10-341-2016
922 Harrysson Drotz, S., Tilston, E. L., Sparrman, T., Schleucher, J., Nilsson, M., Öquist, M. G. (2009).
923 Contributions of matric and osmotic potentials to the unfrozen water content of frozen soils.
924 *Geoderma, 148*(3-4), 392-398. https://doi.org/10.1016/j.geoderma.2008.11.007
925 He, H., Flerchinger, G. N., Kojima, Y., Dyck, M., Lv, J. (2021). A review and evaluation of 39 thermal
926 conductivity models for frozen soils. *Geoderma, 382*, 114694.
927 https://doi.org/10.1016/j.geoderma.2020.114694
928 Hermoso De Mendoza, I., Beltrami, H., MacDougall, A. H., Mareschal, J. (2020). Lower boundary
929 conditions in land surface models – effects on the permafrost and the carbon pools: a case
930 study with CLM4.5. *Geoscientific Model Development, 13*(3), 1663-1683.
931 https://doi.org/10.5194/gmd-13-1663-2020
932 Hu, G., Zhao, L., Li, R., Wu, T., Wu, X., Pang, Q., et al. (2015). Modeling hydrothermal transfer
933 processes in permafrost regions of Qinghai-Tibet Plateau in China. *Chinese Geographical*

Science, 25(6), 713-727. https://doi.org/10.1007/s11769-015-0733-6

Hu, G., Zhao, L., Zhu, X., Wu, X., Wu, T., Li, R., et al. (2020). Review of algorithms and parameterizations to determine unfrozen water content in frozen soil. *Geoderma, 368*, 114277. https://doi.org/10.1016/j.geoderma.2020.114277

Huang, M., Gallichand, J. (2006). Use of the SHAW model to assess soil water recovery after apple trees in the gully region of the Loess Plateau, China. *Agricultural Water Management, 85*(1-2), 67-76. https://doi.org/10.1016/j.agwat.2006.03.009

Ji, H., Nan, Z., Hu, J., Zhao, Y., Zhang, Y. (2022). On the spin‐up strategy for spatial modeling of permafrost dynamics: A case study on the Qinghai‐Tibet Plateau. *Journal of Advances in Modeling Earth Systems, 14*(3), e2021M-e2750M. https://doi.org/10.1029/2021MS002750

Kahimba, F. C., Ranjan, R. S., Mann, D. D. (2009). Modeling soil temperature, frost depth, and soil moisture redistribution in seasonally frozen agricultural soils. *Applied Engineering in Agriculture, 25*(6), 871-882. https://doi.org/10.13031/2013.29237

Kane, D. L., Stein, J. (1983). Water movement into seasonally frozen soils. *Water Resources Research, 19*(6), 1547-1557. https://doi.org/10.1029/WR019i006p01547

Kirchner, J. W. (2006). Getting the right answers for the right reasons: Linking measurements, analyses, and models to advance the science of hydrology. *Water Resources Research, 42*(3). https://doi.org/10.1029/2005WR004362

Koren, V., Schaake, J., Mitchell, K., Duan, Q. Y., Chen, F., Baker, J. M. (1999). A parameterization of snowpack and frozen ground intended for NCEP weather and climate models. *Journal of Geophysical Research: Atmospheres, 104*(D16), 19569-19585.

955 Kulik, V. D. (1978). *Water infiltration into soil (in Russian)*. Gidrometeoizdat, Moscow.

956 Kurylyk, B. L., Watanabe, K. (2013). The mathematical representation of freezing and thawing processes
957 in variably-saturated, non-deformable soils. *Advances in Water Resources, 60*, 160-177.
958 https://doi.org/10.1016/j.advwatres.2013.07.016

959 Li, Q., Sun, S., Xue, Y. (2010). Analyses and development of a hierarchy of frozen soil models for cold
960 region study. *Journal of Geophysical Research, 115*(D3), 1-18.
961 https://doi.org/10.1029/2009JD012530

962 Li, R., Zhao, L., Wu, T., Wang, Q., Ding, Y., Yao, J., et al. (2019). Soil thermal conductivity and its
963 influencing factors at the Tanggula permafrost region on the Qinghai-Tibet Plateau.
964 *Agricultural and Forest Meteorology, 264*, 235-246.
965 https://doi.org/10.1016/j.agrformet.2018.10.011

966 Li, X., Wu, T., Zhu, X., Jiang, Y., Hu, G., Hao, J., et al. (2020). Improving the Noah‐MP model for
967 simulating hydrothermal regime of the active layer in the permafrost regions of the Qinghai-
968 Tibet Plateau. *Journal of Geophysical Research: Atmospheres, 125*(16), e2020J-e32588J.
969 https://doi.org/10.1029/2020JD032588

970 Liljedahl, A. K., Boike, J., Daanen, R. P., Fedorov, A. N., Frost, G. V., Grosse, G., et al. (2016). Pan-
971 Arctic ice-wedge degradation in warming permafrost and its influence on tundra hydrology.
972 *Nature Geoscience, 9*(4), 312-318. https://doi.org/10.1038/ngeo2674

973 Link, T. E., Flerchinger, G. N., Unsworth, M., Marks, D. (2004). Simulation of water and energy fluxes
974 in an old-growth seasonal temperate rain forest using the Simultaneous Heat and Water (SHAW)
975 Model. *Journal of Hydrometeorology, 5*(3), 443-457. https://doi.org/10.1175/1525-

7541(2004)005<0443:SOWAEF>2.0.CO;2

Liu, Y., Yang, Z., Lin, P., Zheng, Z., Xie, S. (2020). Comparison and evaluation of multiple land surface products for the water budget in the Yellow River Basin. *Journal of Hydrology, 584*, 124534. https://doi.org/10.1016/j.jhydrol.2019.124534

Liu, Y., Zhao, L., Li, R. (2013). Simulation of the soil water-thermal features within the active layer in Tanggula Region, Tibetan Plateau, by using SHAW model. *Journal of Glaciology and Geocryology, 35*(2), 280-290.

Loh, W. L. (1996). On Latin hypercube sampling. *The Annals of Statistics, 24*(5), 2058-2080. https://doi.org/10.1214/aos/1069362310

Lv, M., Xu, Z., Yang, Z. L., Lu, H., Lv, M. (2021). A comprehensive review of specific yield in land surface and groundwater studies. *Journal of Advances in Modeling Earth Systems, 13*(2). https://doi.org/10.1029/2020MS002270

Mai, J., Craig, J. R., Tolson, B. A., Arsenault, R. (2022). The sensitivity of simulated streamflow to individual hydrologic processes across North America. *Nature Communications, 13*(1). https://doi.org/10.1038/s41467-022-28010-7

Marshall, A. M., Link, T. E., Flerchinger, G. N., Nicolsky, D. J., Lucash, M. S. (2021). Ecohydrological modelling in a deciduous boreal forest: Model evaluation for application in non‐stationary climates. *Hydrological Processes, 35*(6). https://doi.org/10.1002/hyp.14251

Mullins, C. E. (2000). Matric potential. In *In Soil and Environmental Analysis* (pp. 77-106): CRC Press.

Nimmo, J. R. (1991). Comment on the Treatment of Residual Water Content in "A Consistent Set of Parametric Models for the Two-Phase Flow of Immiscible Fluids in the Subsurface" by L.

997 Luckner et al. *Water Resources Research, 27*(4), 661-662. https://doi.org/10.1029/91WR00165

998 Obu, J. (2021). How much of the earth's surface is underlain by permafrost? *Journal of Geophysical*
999 *Research: Earth Surface, 126*(5). https://doi.org/10.1029/2021JF006123

1000 Oleson, K., Lawrence, D. M., Bonan, G. B., Drewniak, B., Huang, M., Koven, C. D., et al. (2013).
1001 *Technical description of version 4.5 of the Community Land Model (CLM)*. Boulder, Colorado:
1002 National Center for Atmospheric Research.

1003 Painter, S. L. (2011). Three-phase numerical model of water migration in partially frozen geological
1004 media: model formulation, validation, and applications. *Computational Geosciences, 15*(1), 69-
1005 85. https://doi.org/10.1007/s10596-010-9197-z

1006 Pan, T., Hou, S., Liu, Y., Tan, Q. (2019). Comparison of three models fitting the soil water retention
1007 curves in a degraded alpine meadow region. *Scientific Reports, 9*(1).
1008 https://doi.org/10.1038/s41598-019-54449-8

1009 Schoups, G., van de Giesen, N. C., Savenije, H. H. G. (2008). Model complexity control for hydrologic
1010 prediction. *Water Resources Research, 44*(12). https://doi.org/10.1029/2008WR006836

1011 Slater, A. G., Lawrence, D. M. (2013). Diagnosing present and future permafrost from climate models.
1012 *Journal of Climate, 26*(15), 5608-5623. https://doi.org/10.1175/JCLI-D-12-00341.1

1013 Smith, S. L., O'Neill, H. B., Isaksen, K., Noetzli, J., Romanovsky, V. E. (2022). The changing thermal
1014 state of permafrost. *Nature Reviews Earth & Environment, 3*(1), 10-23.
1015 https://doi.org/10.1038/s43017-021-00240-1

1016 Stuurop, J. C., van der Zee, S. E. A. T., Voss, C. I., French, H. K. (2021). Simulating water and heat
1017 transport with freezing and cryosuction in unsaturated soil: Comparing an empirical, semi-

empirical and physically-based approach. *Advances in Water Resources, 149*, 103846. https://doi.org/10.1016/j.advwatres.2021.103846

USDA. (2017). *Soil Survey Division Staff; Soil Conservation Service Volume Handbook 18*: USDA.

USDA. (2019). SHAW Model – Version 3.0.2 Release with Graphical User Interface [Software]. https://www.ars.usda.gov/pacific-west-area/boise-id/northwest-watershed-research-center/docs/shaw-model/

van Genuchten, M. (1980). A closed‐form equation for predicting the hydraulic conductivity of unsaturated soils. *Soil Science Society of America Journal, 44*(5), 892-898. https://doi.org/10.2136/sssaj1980.03615995004400050002x

Walvoord, M. A., Kurylyk, B. L. (2016). Hydrologic impacts of thawing permafrost - A review. *Vadose Zone Journal, 15*(6). https://doi.org/doi:10.2136/vzj2016.01.0010

Wang, J., Luo, S., Lv, Z., Li, W., Tan, X., Dong, Q., Chen, Z. (2021). Improving ground heat flux estimation: considering the effect of freeze/thaw process on the seasonally frozen ground. *Journal of Geophysical Research: Atmospheres, 126*(24). https://doi.org/10.1029/2021JD035445

Wang, L., Zhou, J., Qi, J., Sun, L., Yang, K., Tian, L., et al. (2017). Development of a land surface model with coupled snow and frozen soil physics. *Water Resources Research, 53*(6), 5085-5103. https://doi.org/10.1002/2017WR020451

Wang, Q., Yang, Q., Guo, H., Xiao, X., Jin, H., Li, L., et al. (2019). Hydrothermal variations in soils resulting from the freezing and thawing processes in the active layer of an alpine grassland in the Qilian Mountains, northeastern Tibetan Plateau. *Theoretical and Applied Climatology,*

136(3-4), 929-941. https://doi.org/10.1007/s00704-018-2529-y

Watanabe, K., Osada, Y. (2017). Simultaneous measurement of unfrozen water content and hydraulic conductivity of partially frozen soil near 0 °C. *Cold Regions Science and Technology, 142*, 79-84. https://doi.org/10.1016/j.coldregions.2017.08.002

Wei, Z., Jin, H., Zhang, J., Yu, S., Han, X., Ji, Y., et al. (2011). Prediction of permafrost changes in Northeastern China under a changing climate. *Science China Earth Sciences, 54*(6), 924-935. https://doi.org/10.1007/s11430-010-4109-6

Wen, Z., Ma, W., Feng, W., Deng, Y., Wang, D., Fan, Z., Zhou, C. (2012). Experimental study on unfrozen water content and soil matric potential of Qinghai-Tibetan silty clay. *Environmental Earth Sciences, 66*(5), 1467-1476. https://doi.org/10.1007/s12665-011-1386-0

Wu, X., Nan, Z., Zhao, S., Zhao, L., Cheng, G. (2018). Spatial modeling of permafrost distribution and properties on the Qinghai-Tibet Plateau. *Permafrost and Periglacial Processes, 29*(2), 86-99. https://doi.org/10.1002/ppp.1971

Xiao, Y., Zhao, L., Dai, Y., Li, R., Pang, Q., Yao, J. (2013). Representing permafrost properties in CoLM for the Qinghai–Xizang (Tibetan) Plateau. *Cold Regions Science and Technology, 87*, 68-77. https://doi.org/10.1016/j.coldregions.2012.12.004

Xue, K., Wen, Z., Zhu, Z., Wang, D., Luo, F., Zhang, M. (2021). An experimental study of the relationship between the matric potential, unfrozen water, and segregated ice of saturated freezing soil. *Bulletin of Engineering Geology and the Environment, 80*(3), 2535-2544. https://doi.org/10.1007/s10064-020-02052-x

Yang, J., Reichert, P., Abbaspour, K. C., Xia, J., Yang, H. (2008). Comparing uncertainty analysis

techniques for a SWAT application to the Chaohe Basin in China. *Journal of Hydrology, 358*(1-2), 1-23. https://doi.org/10.1016/j.jhydrol.2008.05.012

Yoshida, T., Hanasaki, N., Nishina, K., Boulange, J., Okada, M., Troch, P. A. (2022). Inference of parameters for a global hydrological model: identifiability and predictive uncertainties of climate - based parameters. *Water Resources Research, 58*(2). https://doi.org/10.1029/2021WR030660

Zhang, T., Heginbottom, J. A., Barry, R. G., Brown, J. (2000). Further statistics on the distribution of permafrost and ground ice in the Northern Hemisphere. *Polar geography, 24*(2), 126-131. https://doi.org/10.1080/10889370009377692

Zhang, X., Sun, S. F., Xue, Y. (2007). Development and testing of a frozen soil parameterization for cold region studies. *Journal of Hydrometeorology, 8*(4), 690-701. https://doi.org/10.1175/JHM605.1

Zhao, L., Zou, D., Hu, G., Wu, T., Du, E., Liu, G., et al. (2021). A synthesis dataset of permafrost thermal state for the Qinghai–Tibet (Xizang) Plateau, China. *Earth System Science Data, 13*(8), 4207-4218. https://doi.org/10.5194/essd-13-4207-2021

Zhao, Y., Nan, Z., Ji, H., Zhao, L. (2022). Convective heat transfer of spring meltwater accelerates active layer phase change in Tibet permafrost areas. *The Cryosphere, 16*(3), 825-849. https://doi.org/10.5194/tc-16-825-2022

Zheng, D., van der Velde, R., Su, Z., Wen, J., Wang, X., Yang, K. (2017). Evaluation of Noah frozen soil parameterization for application to a Tibetan meadow ecosystem. *Journal of Hydrometeorology, 18*(6), 1749-1763. https://doi.org/10.1175/JHM-D-16-0199.1

Zhu, X., Wu, T., Hu, G., Ni, J., Zou, D., Chen, J., et al. (2021). Non-negligible contribution to seasonally

1081 thawing depth of active layer from extreme warming events in the Tanggula permafrost region
1082 of Qinghai-Tibet Plateau. *Journal of Geophysical Research: Atmospheres, 126*(17), e2021J-
1083 e35088J. https://doi.org/10.1029/2021JD035088
1084 Zhu, X., Wu, T., Li, R., Xie, C., Hu, G., Qin, Y., et al. (2017). Impacts of summer extreme precipitation
1085 events on the hydrothermal dynamics of the active layer in the Tanggula permafrost region on
1086 the Qinghai-Tibetan Plateau. *Journal of Geophysical Research: Atmospheres, 122*(21), 11549-
1087 11567. https://doi.org/10.1002/2017JD026736
1088 Zou, D., Zhao, L., Sheng, Y., Chen, J., Hu, G., Wu, T., et al. (2017). A new map of permafrost distribution
1089 on the Tibetan Plateau. *The Cryosphere, 11*(6), 2527-2542. https://doi.org/10.5194/tc-11-2527-
1090 2017
1091 Zuo, Y., Guo, Y., Song, C., Jin, S., Qiao, T. (2019). Study on soil water and heat transport characteristic
1092 responses to land use change in Sanjiang Plain. *Sustainability, 11*(1), 157.
1093 https://doi.org/10.3390/su11010157
1094

[Water Resources Research]

Supporting Information for

[Evaluation of parameterization schemes for matric potential in frozen soil in land surface models: A modeling perspective]

[Yi Zhao[1], Zhuotong Nan[1,2*], Zetao Cao[1], Hailong Ji[1], Jianan Hu[1]]

[[1]Key Laboratory of Ministry of Education on Virtual Geographic Environment, Nanjing Normal University, Nanjing, 210023, China

[2]Jiangsu Center for Collaborative Innovation in Geographical Information Resource Development and Application, Nanjing, 210023, China]

Contents of this file

Figures S1 to S6

Introduction

Supplementary Figures are to be used with the main manuscript for showing the distribution patterns of NSE versus the air entry potential ($\boldsymbol{\psi_e}$) (Figures S1 to S2) and pore size distribution ($\boldsymbol{b}$) (Figures S3 to S4) parameters based on valid soil temperature and moisture simulations for each SMP scenario, as well as the 95PPUs of an additional experiment based on Eq.3 while using a smaller value of the parameter $\boldsymbol{C_k}$ of 2 (Figures S5 and S6).

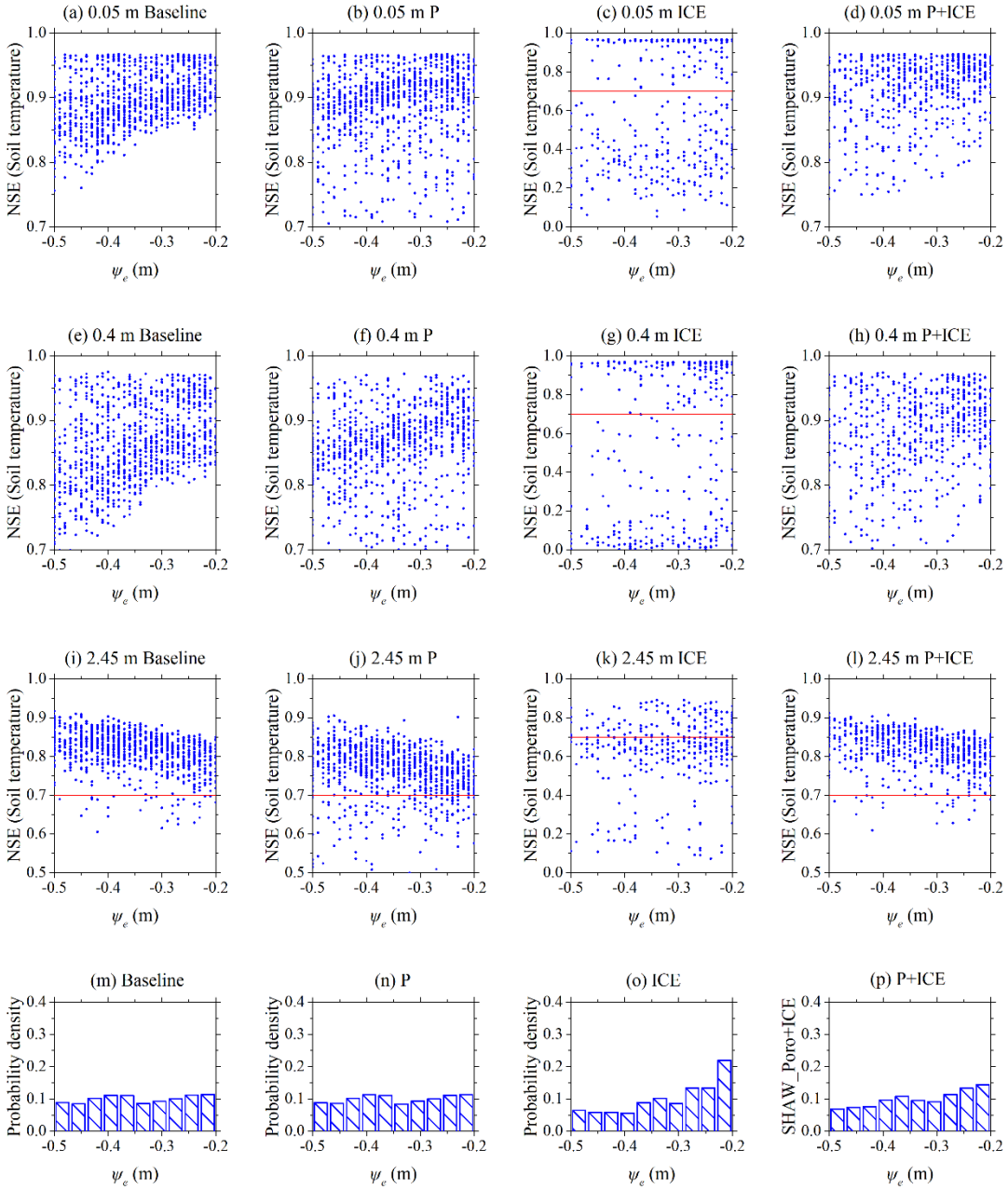

Figure S1. Scatter plots showing the distribution patterns of NSE versus air entry potential (ψ_e) based on valid soil temperature simulations at depths of 0.05 m (a-d), 0.4 m (e-h) and 2.45 m (i-l) for the four scenarios with different SMP schemes in the SHAW model. The probability density distribution of ψ_e for the 0.05 m depth sampled using the Latin hypercube sampling method is shown for each scenario (m-p). Other depths have similar ψ_e sampling distributions and are therefore not shown. The red horizontal lines indicate an NSE value of 0.7, which represents a satisfactory level of simulation accuracy for soil temperature.

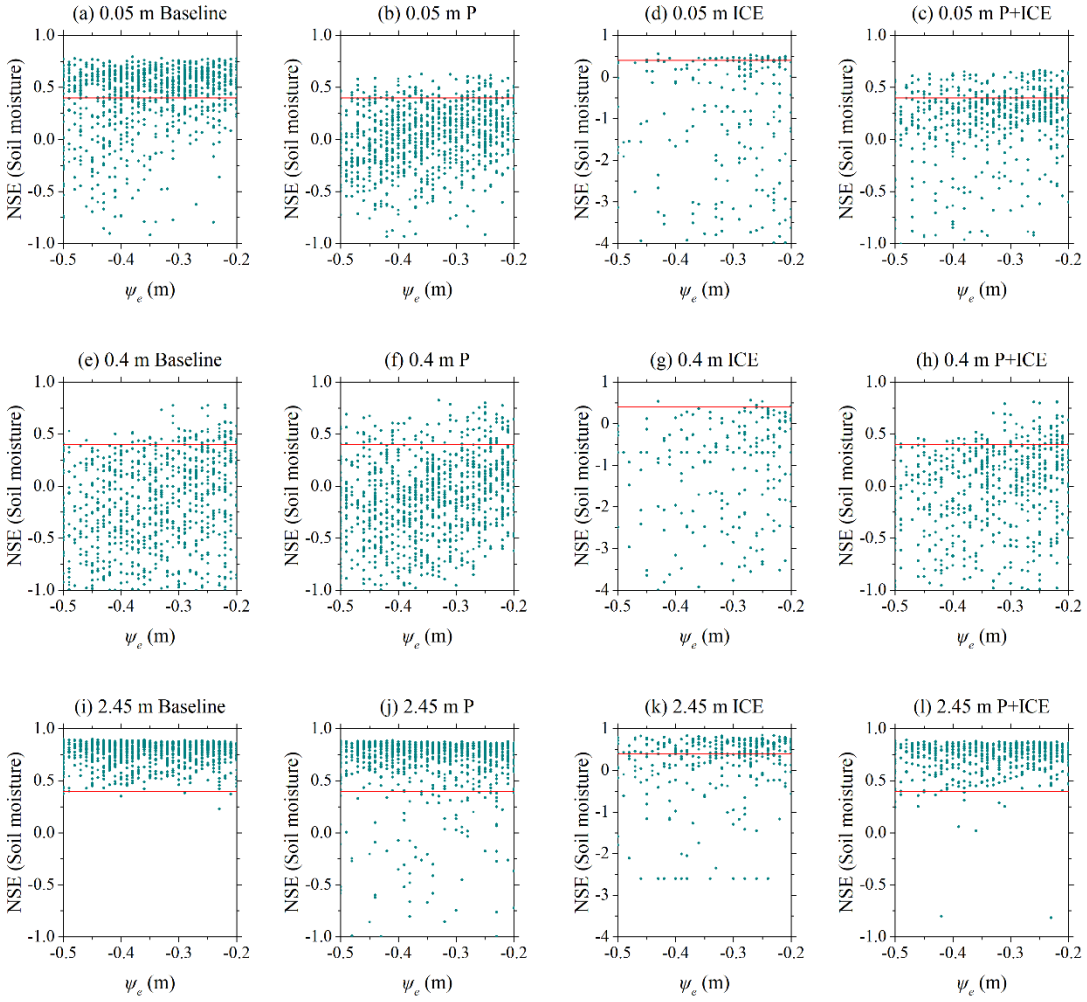

Figure S2. Scatter plots showing the distribution patterns of NSE versus air entry potential (ψ_e) based on valid soil moisture simulations at depths of 0.05 m (a-d), 0.4 m (e-h) and 2.45 m (i-l) for the four scenarios with different SMP schemes in the SHAW model. The probability density distributions of ψ_e are the same as those shown in Figure S1. The red horizontal lines indicate an NSE value of 0.4, which represents a satisfactory level of simulation accuracy for soil moisture.

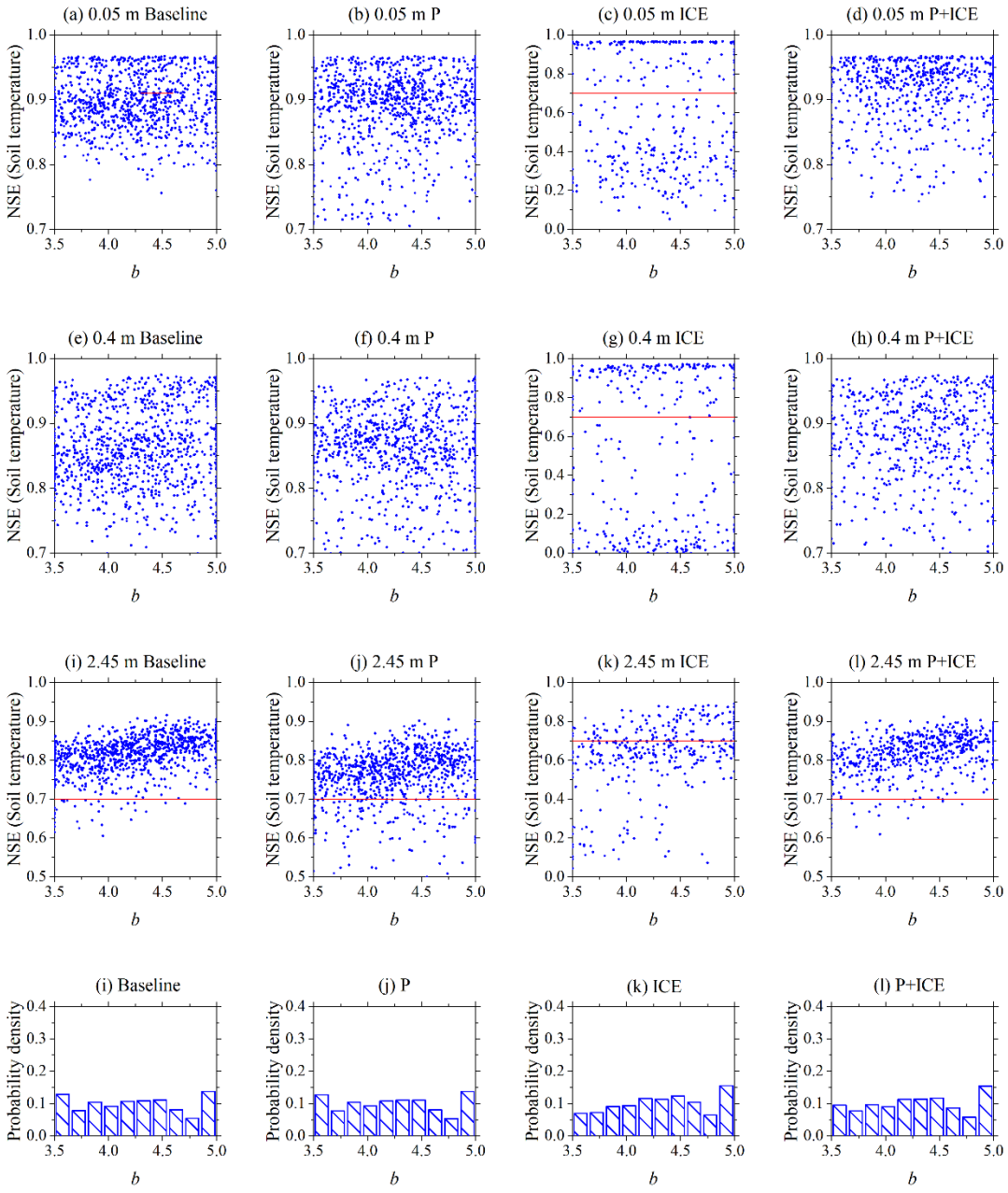

Figure S3. Scatter plots showing the distribution patterns of NSE versus pore size distribution (***b***) based on valid soil temperature simulations at depths of 0.05 m (a-d), 0.4 m (e-h) and 2.45 m (i-l) for the four scenarios with different SMP schemes in the SHAW model. The probability density distribution of ***b*** for the 0.05 m depth sampled using the Latin hypercube sampling method is shown for each scenario (m-p). Other depths have similar ***b*** sampling distributions and are therefore not shown. The red horizontal lines indicate an NSE value of 0.7, which represents a satisfactory level of simulation accuracy for soil temperature.

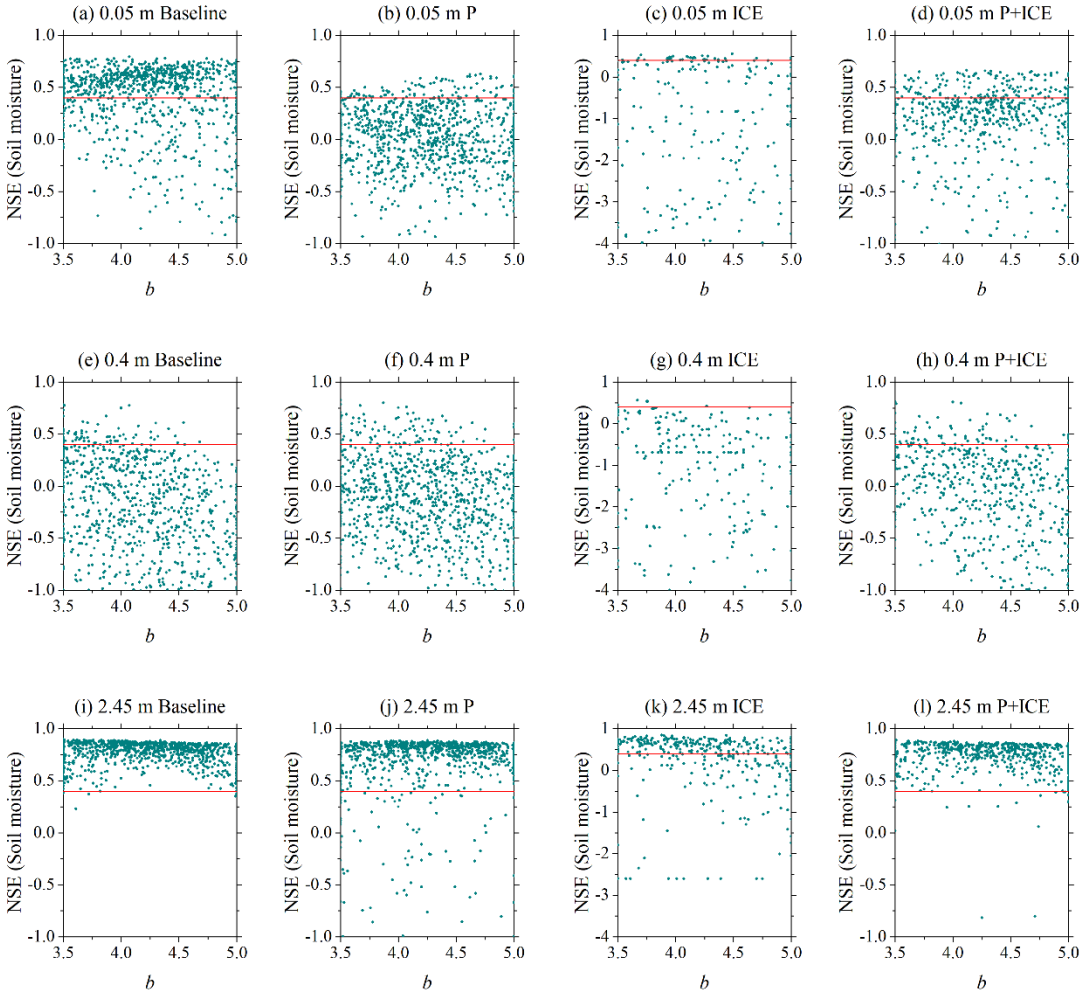

Figure S4. Scatter plots showing the distribution patterns of NSE versus pore size distribution (***b***) based on valid soil moisture simulations at depths of 0.05 m (a-d), 0.4 m (e-h) and 2.45 m (i-l) for the four scenarios with different SMP schemes in the SHAW model. The probability density distributions of ***b*** are the same as those shown in Figure S3. The red horizontal lines indicate an NSE value of 0.4, which represents a satisfactory level of simulation accuracy for soil moisture.

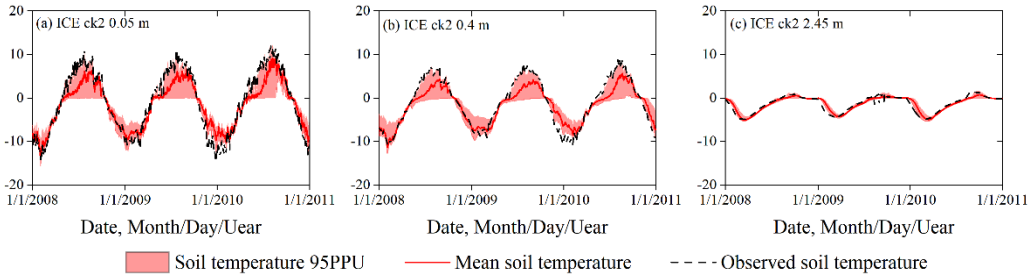

Figure S5. 95 percent prediction uncertainty (95PPU) bands (red shaded areas) for simulated soil temperature at depths of 0.05 m (a), 0.40 m (b) and 2.45 m (c) for an additional scenario, ICE ck2. This scenario is based on Eq.3, where the parameter ck is set to 2. The red solid lines show the means of the simulated soil temperatures based on all valid simulations of each SMP scenario.

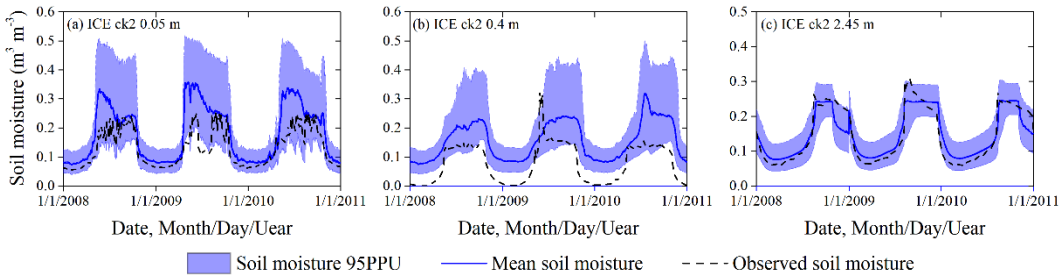

Figure S6. 95PPU bands (blue shaded areas) for simulated soil moisture content at depths of 0.05 m (a), 0.40 m (b) and 2.45 m (c) in the ICE ck2 scenario, which uses Eq.3 with a modified value of ck set to 2. The same notations as in Figure S5 are applied.